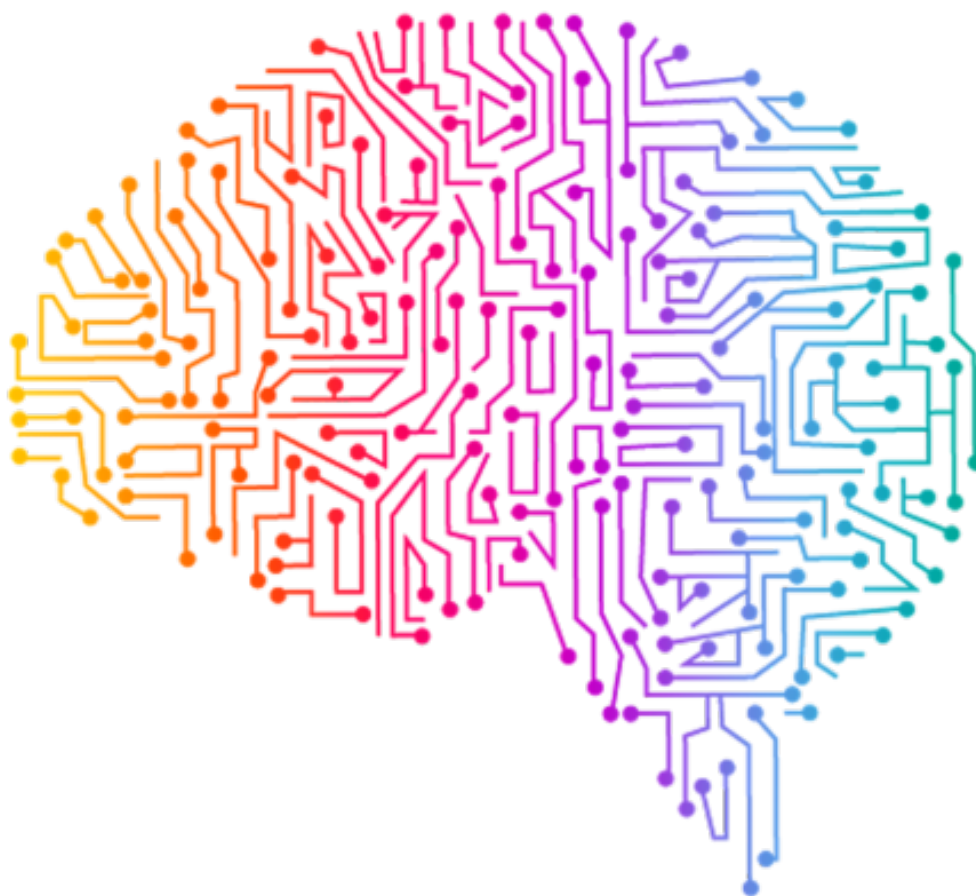

CEREBRAL PERFUSION DURING AORTIC ARCH SURGERY

A THESIS SUBMITTED FOR THE MASTER'S DEGREE IN TECHNICAL MEDICINE

by Eva Cindel Albers



Faculty of Science and Technology

University of Twente

December 2022

ABSTRACT

Introduction – Aortic arch surgery has a high risk of post-operative neurological deficits. In patients with increased risk of neurological complications, the importance of perioperative neuromonitoring increases. Several mechanisms play a role in the pathophysiology of post-surgery neurological complications. A mismatch between cerebral oxygen supply and demand is considered to be one of the most important pathways that can lead to cerebral ischemia, with neurological deficits as a result. In order to evaluate the impact of the multiple pathophysiological processes influencing cerebral blood flow and metabolism simultaneously, a multimodal approach is necessary. The aim of the study was to test feasibility of a multimodal peri-operative test set-up, and to measure cerebral supply and demand during and after aortic arch surgery.

Methods - In this study cerebral supply and demand parameters will be monitored with Near-infrared Spectroscopy (NIRS), Electroencephalography (EEG), Transcranial Doppler (TCD) and jugular venous oximetry. Besides feasibility of the multi-modal approach, the primary outcome in this thesis is the cerebral supply and demand parameters over time from the start of surgery until the moment of awakening at the ICU. Regulatory mechanisms, i.e., cerebral autoregulation and neurovascular coupling, are evaluated through measures as Mean Flow Index (Mx), Cerebral Oximetry index (COx) and Modulation Index (MI).

Results - Four patients were included in this study, of which one patient developed a delirium. Mean arterial pressure and mean flow velocity in the middle cerebral artery increased from surgery to ICU while relative power in the delta band decreased. The results showed a high interpatient variability in the cerebral supply and demand parameters. Mx and COx reported moments of impaired cerebral autoregulation, but not simultaneously.

Discussion – In this study we have shown feasibility of multimodal neuromonitoring during aortic arch surgery. The method described in this study facilitates simultaneous analysis of multiple cerebral hemodynamic regulatory mechanisms. Issues regarding synchronization of the data collected in ICM+ remain to be solved.

GRADUATION COMMITTEE

Chairman and technical supervisor – prof.dr. R.J.A. van Wezel (University of Twente)

Clinical supervisor – dr. C.W.E. Hoedemaekers (Radboudumc Nijmegen)

Supervisor personal development – drs. P.A. van Katwijk (University of Twente)

Additional member – C.R. van Kaam, MSc (Radboudumc Nijmegen)

External member - M.M.L.H. Verhulst, MSc (University of Twente)

LIST OF ABBREVIATIONS

ICU – intensive care unit	rSO ₂ – regional saturation
MAP – mean arterial pressure	HHb – deoxygenated hemoglobin
spO ₂ – peripheral saturation	TSI – tissue saturation index
BP – blood pressure	OEF – oxygen extraction fraction
ECC – extracorporeal circulation	EEG – electroencephalogram
TCD – Transcranial Doppler	MI – Modulation Index
CBF – cerebral blood flow	NVC – neurovascular coupling
CBFV – cerebral blood flow velocity	CFC – cross-frequency coupling
MFV – mean flow velocity	Mx – Mean flow index
NIRS – Near-Infrared spectroscopy	COx – cerebral oximetry index
Hb – hemoglobin	S _{vj} O ₂ – jugular bulbus oxygen saturation
O ₂ Hb – oxygenated hemoglobin	PND – post-neurological disorder

TABLE OF CONTENTS

1	INTRODUCTION	6
1.1	MULTIMODAL MONITORING.....	8
	<i>Transcranial doppler</i>	9
	<i>Near Infrared Spectroscopy</i>	9
	<i>EEG</i>	10
	<i>Jugular Venous Oximetry</i>	10
1.2	REGULATORY MECHANISMS OF CEREBRAL BLOOD FLOW	11
	<i>Cerebral Autoregulation</i>	11
	<i>Neurovascular coupling</i>	12
2	METHODS	13
2.1	DATA ACQUISITION	13
	<i>Synchronization</i>	14
2.2	DATA PREPROCESSING.....	15
	<i>ICM+ dataset</i>	15
	<i>EEG dataset</i>	17
2.3	DATA ANALYSIS	17
	<i>Cerebral supply and demand parameters over time</i>	18
	<i>Regulatory Mechanisms of Cerebral Blood Flow</i>	18
3	RESULTS	21
3.1	FEASIBILITY	21
3.2	CEREBRAL SUPPLY AND DEMAND OF BLOOD AND OXYGEN	23
3.3	REGULATORY MECHANISMS OF CEREBRAL BLOOD FLOW	28
	<i>Cerebral Autoregulation</i>	28
	<i>Neurovascular Coupling</i>	29
3.4	SYNCHRONIZATION PROBLEM.....	30
4	DISCUSSION	32
4.1	FEASIBILITY OF THE STUDY	32
4.2	RESULT INTERPRETATION	33
	<i>Cerebral supply and demand parameters</i>	33
	<i>Post neurological deficits</i>	35
4.3	LIMITATIONS & RECOMMENDATIONS	36
5	CONCLUSION	37
6	REFERENCES	38
7	APPENDIX	42

7.1 EEG INFLUENCED BY ECC 42

1 INTRODUCTION

Despite all advances in anesthesia and cardiac surgery, aortic arch surgery is still associated with high rates of brain injury.¹ Additionally, as life-expectancy increases, more elderly patients are presenting for cardiac surgery.^{2,3} Due to the combination of advanced age and risk of brain injury caused by aortic arch surgery, the frequency of post-operative neurological deficits (PND) increases.⁴ The complications can range from agitation or delirium to more permanent complications including stroke or coma. Delirium after aortic arch surgery has a reported incidence of 13-25% and is known to increase costs, length of stay in the hospital and mortality.^{5,6,7}

The aortic arch is the origin for the vessels supplying blood to the brain.⁸ Aneurysms of the aortic wall often develop over the course of many years with little to no symptoms. However, left untreated the risk of dissection increases, which is life threatening.⁸ During aortic arch surgery, aneurysms or dissections are treated with partial or complete replacement of the aortic arch. Aortic arch surgery is a technically advanced procedure and, depending on the location of the repair, usually requires extracorporeal circulation (ECC) and circulatory arrest. Even though the pathophysiology of the neurological deficits such as delirium is multi-factorial, it is believed that inadequate cerebral perfusion is a major component.⁹

The functionality and survival of neurological tissue completely depends on its blood supply since the brain has a limited inherent energy and oxygen source.^{10,11} The brain has multiple regulatory hemodynamic mechanisms ensuring adequate perfusion at all times. Two important mechanisms are cerebral autoregulation and neurovascular coupling. As the brain is sensitive to hypoxia, an impairment in the supply of oxygen and nutrients can lead to cellular damage or even cell death.¹² A mismatch between cerebral oxygen supply and demand can lead to cerebral ischemia, with neurological deficits as a result. In an attempt to match the possible decrease in supply of oxygen and nutrients, anesthesia and hypothermia decrease the cerebral metabolic rate of oxygen during the procedure. However, it remains unknown whether the change in cerebral activity during and after the procedure is proportional to the changes in cerebral perfusion. For this reason, it is unknown whether the cerebral supply and demand is in balance in the period from surgery to the moment of awakening at the ICU.

In order to evaluate the impact of the multiple physiological processes influencing cerebral blood flow (CBF) simultaneously, a multimodal approach is necessary. The multimodal approach used in this study will include Near-infrared Spectroscopy (NIRS), Electroencephalography (EEG), Transcranial Doppler (TCD) and jugular venous oximetry. In order to evaluate whether the perfusion of the brain is adequate or not, the balance between supply and demand was analyzed. A schematic overview of the parameters involved in the balance between cerebral supply and demand is provided in figure 1. Parameters such as regional saturation and cerebral blood flow reflect cerebral supply, whereas electrocortical activity

reflects cerebral demand. The balance between supply and demand may be assessed through the regional and global oxygen extraction of the brain.

In this thesis we aimed to demonstrate possible changes in the balance between cerebral supply and demand during and after aortic arch surgery.

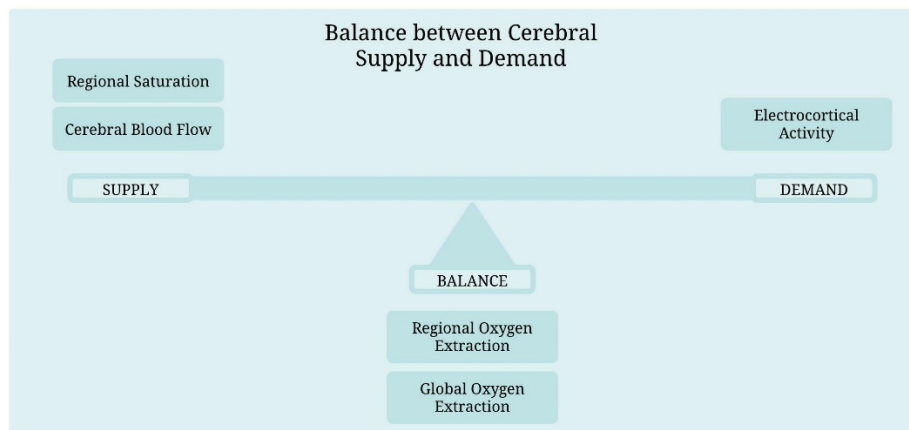


Figure 1: A schematic overview of the parameters involved in the balance between cerebral supply and demand.

1.1 MULTIMODAL MONITORING

As there is no single definitive neuromonitor, cerebral perfusion and oxygenation was assessed with the use of several modalities. An overview of the neuromonitoring modalities used in this study is provided in table 1.¹³

Table 1: Overview of neuromonitoring modalities used in this study, with physiological parameter, technique, advantages and disadvantages and parameter used in this study.

NEUROMONITORING MODALITIES

MODALITY	Physiological parameter	Technique	Advantage	Disadvantage	Parameter used
Transcranial doppler (TCD)	Localized cerebral blood flow velocity and direction	Noninvasive; probes are placed bilaterally at temporal window	Can detect changes in perfusion as well as emboli	Requires technical skill; operator dependent and sensitive to artifacts	Mean Cerebral Blood Flow Velocity in the Middle Cerebral Artery (MFV_{MCA}) Cerebral autoregulation (Mx)
Near Infrared Spectroscopy (NIRS)	Regional cerebral oxygen saturation	Noninvasive; adhesive device is placed on frontal region	Simple interpretation, easily placed and can detect regional desaturation	Regional measurement, poor inter-changeability of devices. Reliability discussed due to potential of extracranial contamination	Tissue Saturation Index (TSI) Regional Oxygen Extraction Fraction (OEF_{NIRS}) Cerebral autoregulation (COx)
Electro-encephalogram (EEG)	Global superficial cortex electrical activity	Noninvasive; adhesive electrodes are placed according to the 10-20 system.	Evaluation of cerebral activity and can be used to detect global/regional ischemia.	Monitor of superficial layer. Interpretation relies on skill or algorithm	Relative power in respective frequency bands Modulation Index (MI)
Jugular venous oximetry	Global cerebral oxygenation	Invasive; sited in jugular bulb	Permits evaluation of blood directly from cerebral tissue. High specificity for ischemia.	Global measurement; interpretation of cause of abnormal oxygenation is complex.	Jugular Venous Oxygen saturation ($S_{vj}O_2$) Global oxygen extraction Fraction (OEF_{vj})

Transcranial doppler

TCD can monitor the cerebral blood flow velocity (CBFV) in the middle cerebral artery (MCA). The CBFV is commonly used as an estimate for cerebral blood flow, assuming the diameter of the middle cerebral artery remains constant.^{14,15} The ultrasonic beam is reflected by the erythrocytes in the cerebral vessels and results in a change of frequency.¹⁶ This change of frequency is directly proportional to the velocity of the erythrocytes. The advantage of TCD is the non-invasive and continuous nature of the device. Due to the fact that middle cerebral artery collects nearly 60–70% of the internal carotid arteries blood flow, the evaluation is used to represent the blood flow to one hemisphere. There are many physiological factors which can influence the CBFV, for example age, gender and concentration of CO₂.¹⁷ Additionally, TCD monitoring requires technical skill to find correct insonation window and signal can be easily lost due to movement of the probe.¹³

From the CBFV signal the mean velocity can be derived following the formula:

$$MFV_{MCA} = \frac{\text{peak systolic velocity} + (\text{end diastolic velocity} * 2)}{3} \quad (1)$$

Near Infrared Spectroscopy

NIRS can reflect the changes in local cerebral blood flow and volume by noninvasively measuring the changes in oxygenated, deoxygenated and total hemoglobin (Hb). The near infrared light is absorbed by the oxygenated and deoxygenated hemoglobin (O₂Hb and HHb) chromophores at 780 and 850 nm, respectively. This absorption of light can be converted into a tissue concentration using the modified Lambert-Beer law.¹¹ One of the parameters that can be obtained is the regional cerebral oxygen saturation (rSO₂) measured as the Tissue Saturation Index (TSI).¹⁸ This parameter describes the ratio of O₂Hb to total Hb, calculated as

$$TSI = \frac{O_2Hb}{O_2Hb + HHb} \quad (2)$$

By comparing the TSI to the peripheral oxygen saturation (spO₂), it is possible to estimate the regional oxygen extraction fraction (OEF_{NIRS}) with

$$OEF_{NIRS} = \frac{spO_2 - TSI}{spO_2} \quad (3)$$

An advantage of calculating the oxygen extraction using NIRS, is the ability to continuously monitor and analyze trends. However, when using NIRS, the parameter only reflects regional oxygen extraction and can be influenced by the perfusion of extracerebral tissue.¹³ Moreover, the OEF_{NIRS} cannot be used as an absolute value.¹⁹

EEG

The EEG reflects the extracellular currents between the neurons resulting from the synchronous post-synaptic currents, which makes it a useful tool for the detection of brain activity. An EEG signal consists of a continuous recording of waves with varying frequency and amplitudes. The frequency of the waves describes the firing pattern of the neurons of the cerebral cortex and are associated with different behavioral and neurophysiological states.²⁰ The analysis of the waveforms can be used to indicate the depth of anesthesia during surgery, but also for the detection of cerebral ischemia.^{21,22} In general, reduced oxygen delivery will result in a slowing of the EEG rhythm.²³ As cortical synaptic activity is sensitive to hypoxia, the EEG can also be used to detect cerebral damage induced by hypoxia.^{24,25}

The frequency content of the EEG signal is divided in five frequency bands; δ (0-4 Hz), θ (4-8 Hz), α (8-16 Hz), β (16-32 Hz), γ (>32 Hz). The administration of anesthetics will slow down the EEG signal and decrease amplitude. Slowing down of EEG signal is demonstrated as an increase in relative power in the lower frequencies with a concurrent decrease in relative power in the higher frequencies.²⁶ The relative frequency band power was calculated for all frequency bands according to:

$$EEG \text{ band power } (\gamma, \beta, \alpha, \theta, \delta) = \frac{\text{Frequency bandpower } (\gamma, \beta, \alpha, \theta, \delta)}{\text{Total frequency power}} \quad (4)$$

Jugular Venous Oximetry

Jugular venous oximetry can provide insight in the global oxygenation of the brain. A catheter is inserted retrogradely in the jugular bulb, using a Seldinger technique.²⁷ Sampling of blood from the jugular bulb catheter permits blood gas analysis of venous blood draining from the brain. Jugular venous oximetry enables indirect assessment of the balance between cerebral supply and demand. When cerebral demand exceeds supply, jugular venous oxygen saturation ($S_{Vj}O_2$) decreases as oxygen extraction increases. Jugular venous oximetry is known for its high specificity for ischemia, but has low sensitivity and interpretation of results can be complex.^{13,28}

Using the samples obtained by the jugular bulb catheter provides us with the possibility to analyze parameters such as lactate, hemoglobin and CO_2 concentration. The content of arterial (C_aO_2) and jugular venous ($C_{Vj}O_2$) oxygen are calculated according to the following equations,

$$C_aO_2(ml * dl^{-1}) = [Hb] * 1.36 * \frac{S_aO_2(\%)}{100} + 0.003 * P_aO_2 \quad (5)$$

$$C_{Vj}O_2(ml * dl^{-1}) = [Hb] * 1.36 * \frac{S_{Vj}O_2(\%)}{100} + 0.003 * P_{Vj}O_2 \quad (6)$$

with 1.36 as the constant describing the amount of oxygen bound per gram of hemoglobin and the constant 0.003 representing the amount of oxygen dissolved in plasma.

Comparing the oxygen concentration in the jugular venous sample to the oxygen concentration in the arterial sample enables evaluation of global oxygen extraction fraction. The global oxygen extraction fraction ($OE_{F_{VJ}}$) can be calculated with

$$OE_{F_{VJ}} = \frac{C_a O_2 - C_{VJ} O_2}{C_a O_2} \quad (7)$$

1.2 REGULATORY MECHANISMS OF CEREBRAL BLOOD FLOW

To provide the brain with a constant supply of oxygen and nutrients, cerebral hemodynamics are tightly regulated by many different mechanisms.²⁹ In this thesis we focus on cerebral autoregulation and neurovascular coupling. The multimodal monitoring nature of this study enables the evaluation of these regulatory mechanisms and their interaction.

Cerebral Autoregulation

Cerebral autoregulation refers to the ability of the cerebral vasculature to maintain a constant cerebral perfusion despite blood pressure changes.²⁹ Under normal circumstances, cerebral blood flow is regulated by changes in arteriolar diameter, leading to changes in vascular resistance. This active control of cerebrovascular resistance secures a stable CBF despite changes in arterial blood pressure. If cerebral autoregulation is disturbed, cerebral perfusion will passively follow changes in arterial blood pressure (ABP). When this happens, the brain becomes more vulnerable to ischemia when ABP is low and vulnerable to hyperperfusion and edema when ABP is high. The function of cerebral autoregulation can be assessed in the time domain as the correlation between the mean arterial pressure (MAP) and CBFV or TSI.

The correlation between the MAP and CBFV signal measured with TCD is referred to as the mean flow index (Mx). The correlation between the MAP and TSI measured with NIRS is referred to as the cerebral oximetry index (COx). Both correlations, Mx and COx, can vary between -1 and 1. A positive correlation, close to 1, means that the CBFV or TSI passively follow fluctuations in ABP, indicating impaired cerebral autoregulation. A correlation of zero or negative values indicate active cerebral autoregulation as changes in blood pressure are not followed by CBFV or TSI. In literature a correlation above 0.45 is considered to reflect impaired cerebral autoregulation.³⁰

Neurovascular coupling

Neurovascular coupling (NVC) describes the change in local CBF in response to a change in local neural activity and describes the temporal and regional link between blood flow and activity. When neuronal activity increases in a specific region, this region will receive an increase in cerebral blood flow due to both chemical signals and mechanical effects. The neurovascular unit is a complex structure, consisting of endothelial cells, neurons, smooth muscle cells, pericytes and astrocytes. The cells of the neurovascular unit sense changes in local neuronal activity and causes changes in local blood flow, mediated by transmission through the astrocyte.³¹ In the absence of active NVC, an increase of neuronal activity will not be met by an increase in cerebral blood flow. Hence, cerebral supply and demand will be out of balance, with possible neurological complications as a result.

Currently, NVC is not monitored during surgery, even though the use of circulation manipulation techniques such as ECC likely influences NVC³² The gold standard for NVC evaluation are imaging techniques such as BOLD-MRI or PET.³³ Since these techniques are not feasible during surgery, the possible use of other techniques, such as EEG have gained increasing interest in literature. Recently, Liu et al. described a novel metric for the monitoring of neurovascular coupling by calculating the cross-frequency coupling (CFC) between the EEG signal and CBFV signal measured with TCD in stroke patients.³⁴ Cross frequency coupling describes the interaction between low frequency and high frequency signal oscillations and can be evaluated with the use phase-amplitude coupling. The preliminary work of Liu et al. (2019) is based on the idea that the amplitude of the EEG signal (the high frequency signal) is linked to the phase of the CBFV signal (the low frequency signal). They define this coupling as the modulation index (MI), a metric reviewed most suitable for CFC.^{34,35}

2 METHODS

This is an ongoing observational study including adult patients undergoing elective aortic arch surgery. Exclusion criteria are a rescue or emergency procedure, history of neurological disease (known to influence cerebral blood flow and oxygenation) and failure to obtain informed consent. Since this is a pilot study, the first analysis will be performed after inclusion of ten patients. The protocol of this study was approved by the CMO and registered as file NL76089.091.20.³⁶ In this thesis we present the results of the first four patients included in this study.

The primary outcome in this thesis was feasibility of the multimodal measurements. In addition, parameters reflecting cerebral supply and demand over time and their interaction was measured. In this thesis, cerebral supply was evaluated with the MFV_{MCA} , TSI and mean arterial pressure (MAP). The cerebral demand was evaluated by relative frequency bands of the EEG signal and the cerebral balance was illustrated by the oxygen extraction fraction measured using NIRS (OEF_{NIRS}) and the jugular bulb blood samples (OEF_{VJ}).

The secondary objective of the larger ongoing study will be to evaluate the difference in cerebral perfusion between patients with and without PND. Therefore, the neurological outcome of the subjects is assessed by the incidence of delirium following the Intensive Care Delirium Screening Checklist (ICDSC) criteria.³⁷ The severity of delirium will be described by the number of days with a minimal score of 1 on the ICDSC test.

2.1 DATA ACQUISITION

Measurements were performed during the preoperative consultations, during surgery and at the ICU, see figure 2. In this thesis, we focus on the measurements during surgery and at the ICU. Demographic and clinical data were collected.

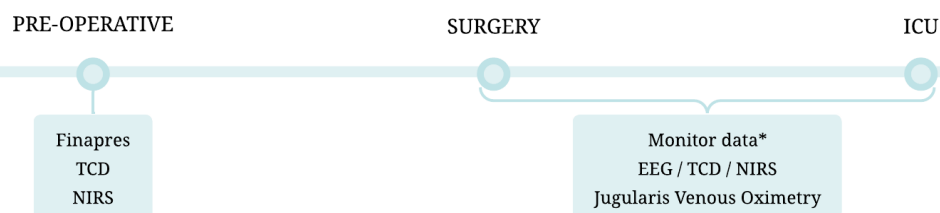


Figure 2: A timeline displaying which measurement techniques will be used during the patient's stay in the hospital. TCD = transcranial doppler, NIRS = near infrared spectroscopy, EEG = electroencephalogram, ICU = intensive care unit.

* Monitor data refers to standard clinical measurements of continuous peripheral oxygen saturation (spO_2) and arterial blood pressure (ABP).

The multimodal monitoring of the intra- and post-operative measurements were performed with the use of the EEG, NIRS, TCD, jugular venous oximetry and monitor data. The monitor data refers to the parameters collected and displayed on the Philips IntelliVue bedside monitor. In this thesis we collected the values for spO_2 and ABP (measured in the radial artery).

The NIRS signal was recorded with the use of the PortaLite device (Artinis medical systems, Elst, the Netherlands) and the Oxysoft program (3.0.103.3, Artinis Medical Systems, Elst, The Netherlands).

The transcranial doppler measurement was performed using a Multi-Dop T device (DWL, Compudemics Germany GmbH). Two 2 MHz probes were placed bilaterally on the temporal bone window and fixated on a head frame. The ideal depth for $CBFV_{MCA}$ evaluation was 45-60mm.^{38,39}

The EEG was recorded in the Brain RT program. Nine silver-chloride cup electrodes were placed on the scalp following the international 10-20 system (O1, O2, T3, C3, Cz, C4, T4, F1 & F2). Due to the placement of the INVOS, BIS and Portalite electrodes on the forehead, it was impossible to use electrodes at the FP1 and FP2 position. For this reason, we chose the F1 and F2 position.

Blood from the jugular bulb was sampled from a 7-Fr single-lumen catheter inserted with the tip into the jugular bulb. Monitoring of blood pressure and arterial blood sampling was performed with the use of a catheter in the radial artery. This catheter, and a central venous catheter, were inserted at the operating theatre and were part of the standard perioperative care. Blood samples from the jugular bulb-, central venous- and arterial catheter were collected and analyzed at the start of induction, during ECC, end of surgery, upon admission at the ICU and at 20:00PM, 00:00AM and 06:00AM the next morning.

Synchronization

The data from the different monitoring devices was simultaneously collected in one file via the Intensive Care Monitor software (ICM+, Cambridge Enterprise, University of Cambridge, U.K.). The data from the IntelliVue monitor was imported with the use of a RS232 cable. The waveforms from the TCD and NIRS devices were directly imported in ICM+ as the respective programs run on the same computer as the ICM+ program. The TSI parameter was calculated in the Oxysoft program retrospectively, meaning that this parameter could not be imported real-time. Furthermore, the EEG was recorded on a separate computer and could not be imported in ICM+ through one of the modalities described above. For this

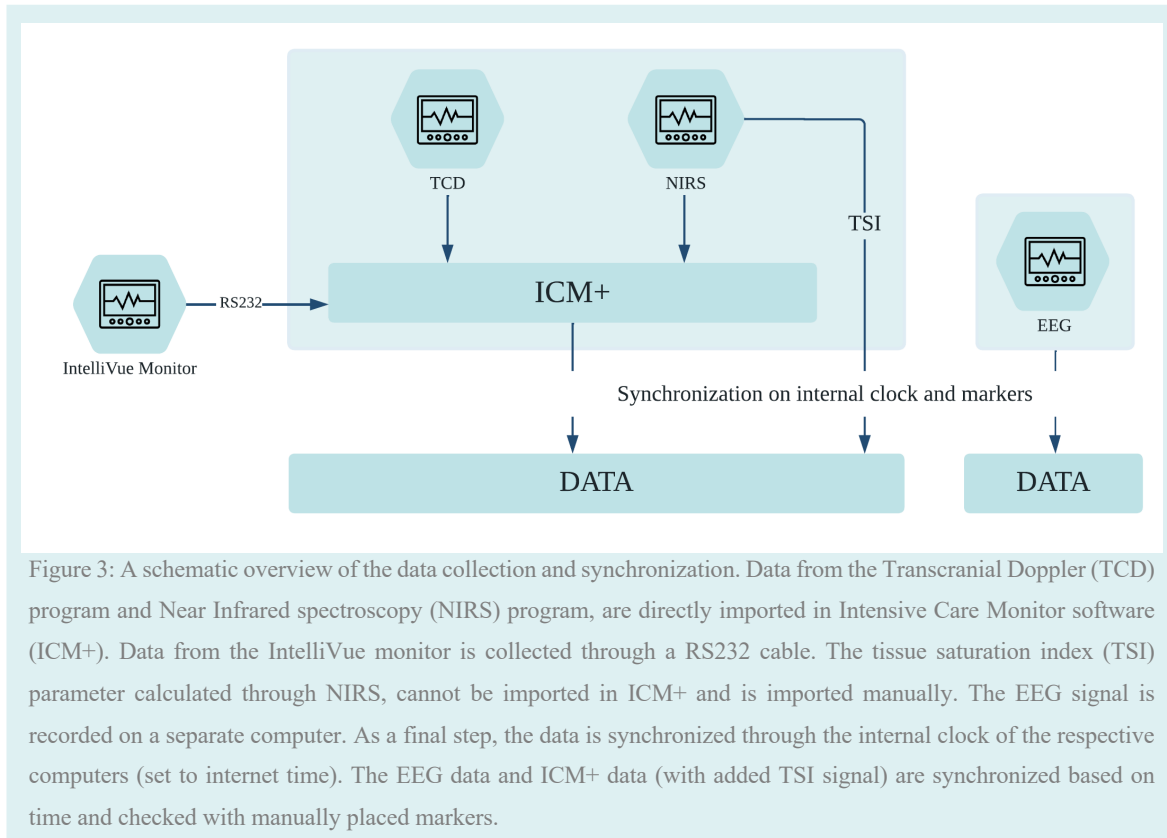


Figure 3: A schematic overview of the data collection and synchronization. Data from the Transcranial Doppler (TCD) program and Near Infrared spectroscopy (NIRS) program, are directly imported in Intensive Care Monitor software (ICM+). Data from the IntelliVue monitor is collected through a RS232 cable. The tissue saturation index (TSI) parameter calculated through NIRS, cannot be imported in ICM+ and is imported manually. The EEG signal is recorded on a separate computer. As a final step, the data is synchronized through the internal clock of the respective computers (set to internet time). The EEG data and ICM+ data (with added TSI signal) are synchronized based on time and checked with manually placed markers.

reason, both the TSI parameter and the EEG signal were synchronized retrospectively, based on local area network time and manually placed markers in the respective datasets. As a result, we had an ICM+ dataset and an EEG dataset, synchronized with precision on the level of seconds. An overview of the data collection is shown in figure 3.

2.2 DATA PREPROCESSING

All data was preprocessed and analyzed using Python 3.8.8 (Python Software Foundation, Wilmington, Delaware, United States).

In order to have a common sample frequency across all signals, all data in the ICM+ dataset was resampled to 125 Hz. The NIRS data was recorded with a sample frequency of 50Hz, whereas the ABP signal was recorded with a sample frequency of 250Hz. This meant that both down and up sampling was needed. Down sampling was performed with the use of the Python `scipy decimate` function whereas the up sampling of data was performed with the use of the Python `scipy interp1d` function.⁴⁰ The EEG dataset had an original sample frequency of 256Hz and is resampled to 128 Hz.

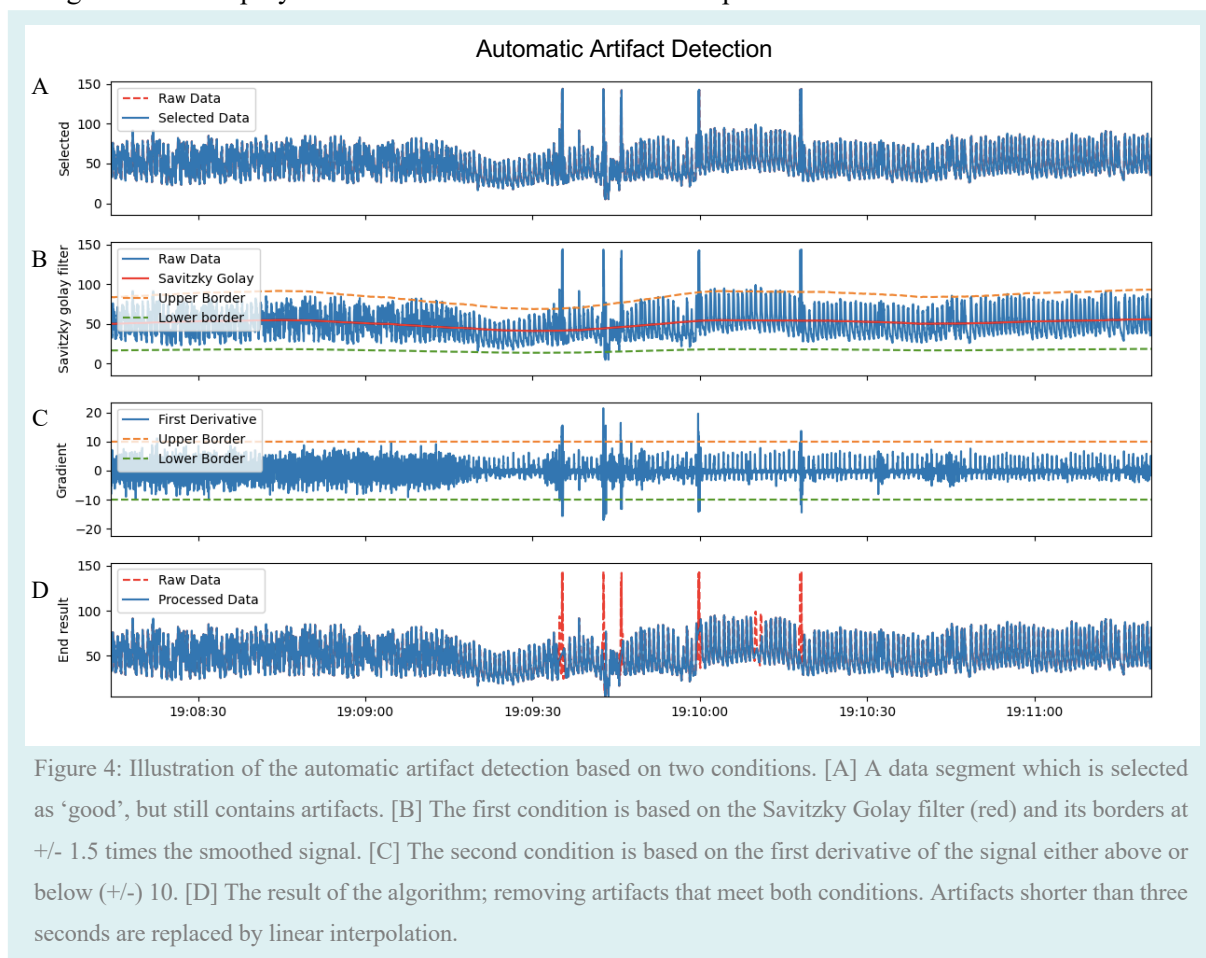
ICM+ dataset

The data consisted of two recordings per patient, one during surgery and one at the ICU. To ensure a correct timeline, the first step was to reintroduce the gap in recording between the stop and restart of measurement, which was filled with NaN values. Additionally, the ICM+ file contained multiple short

recording stops, either caused by an error inside the ICM+ program or an error in the import process of the TCD, NIRS or monitor data. Likewise, these gaps were reintroduced and filled with NaN values.

All data was filtered with a 50Hz notch filter. Visual inspection of the data led to the observation that all data was prone to artefacts and loss of signal, most notably the TCD signal. To ensure quality of data and in order to obtain an overview of artifact free data, we visually inspected the TCD signal in the ICM+ dataset and selected artefact free data with at least one TCD signal of adequate stability. As a result of this manual selection procedure, segments containing large artifacts or loss of data in the TCD signal were eliminated and remaining segments were defined as quality recordings. The segments of TCD data which were not selected were classified as substandard and replaced by NaN values. This step only involved TCD data, meaning that the artifacts in the other signals were still present. Additionally, the selection of data resulted solely in elimination of larger artifacts, whereas small artifacts were still present.

Next, the remaining artifacts were detected through a manually built automatic artifact detection as illustrated in figure 4. Artifacts were characterized by a deviating absolute value and a rapid increase or decrease of the signal. For this reason, the preprocessing steps for artifact elimination included a Savitzky Golay filter and a first derivative signal. The Savitzky Golay filter smoothed the signal by fitting a third order polynomial with a window of 10000 samples. The borders were set at ± 1.5 times



the smoothed signal. In this algorithm, a data segment was recognized as artifact when it met two conditions: an absolute value outside the Savitzky Golay borders and a gradient above or below ± 10 . The combination of the constants at 1.5 and 10 was determined best, based on visual inspection. Similar to the manual selection of data, the data segments marked as artifacts were set to NaN. After these pre-processing steps the data contained multiple segments of NaN values. For the segments shorter than 3 seconds, the data was filled with linear interpolation. Remaining segments are ignored and remained as NaN values.

EEG dataset

Whereas the ICM+ program marked the gaps in the data, this was not seen in the EEG data set. The EEG recording of the ICU measurement was directly appended to the recording in the operation room, without any markers of a pause in the recording. In order to synchronize the EEG data to the other data, this gap had to be re-introduced. Besides the EDF file which contained the EEG signals, the analysis result XML file was exported in order to obtain the exact moment in time where the first recording was stopped, and the second recording was started.

The raw data in the EEG dataset was re-referenced in a bipolar longitudinal montage. Similar to the data collected in ICM+ the gap in the measurement during the transport from the OR to the ICU needed to be re-introduced. Next, all impedance checks were removed, and the data was filtered with a bandpass filter with a low cut-off value of 0.5 Hz and a high cut-off value of 45 Hz. Afterwards, the ECG and EOG artifacts were eliminated with the use of a two-stage adaptive filter based on the method of Correa et al (2007).⁴¹

2.3 DATA ANALYSIS

In this thesis we were interested in the question whether the parameters (MAP, MFV_{MCA} , TSI, OEF_{NIRS} , OEF_{VJ} and EEG activity), and their relation to each other, differ over the course of time from surgery until the next morning at the ICU. The supply parameters included MAP, TSI and MFV_{MCA} . The balance parameters included the regional and global oxygen extraction measured with NIRS (OEF_{NIRS}) and the blood sampled from the jugular bulb (OEF_{VJ}), respectively. The demand parameter was illustrated as the relative power of the frequency bands of the EEG signal. The parameters were calculated as described in the formulas in the introduction. For the EEG parameter, the frequency content was evaluated with the use of average spectrograms over all channels. The power spectral density was computed according to Welch's method. A Hann window of 20 seconds was chosen in order to obtain a frequency resolution of 0.1 Hz. By moving the Hann window across the signal with an overlap factor of 50% the spectrograms were computed.

Cerebral supply and demand parameters over time

The parameters were evaluated at specific timepoints; start induction, start incision, during ECC, end of surgery, admission at the ICU, 20:00PM, 00:00AM and 06:00AM the next morning. Except for the ‘start induction’ moment, blood samples were taken at these timepoints. Since we want to analyze the relation between parameters, quality data segments with a duration of ten minutes were chosen with the closest possible proximity in time to the moment of blood sampling. Of those data segments the mean and standard deviation for each parameter were calculated.

Parameters evaluated over time and between patients, were presented as median and interquartile range. The relation between OEF_{NIRS} and OEF_{VJ} was calculated through the Pearson correlation coefficient, at the moment of the blood sample moments.

Regulatory Mechanisms of Cerebral Blood Flow

In addition to the behavior of the individual cerebral supply and demand parameters over time, we also assessed the interaction between these parameters. We did this through the quantification of measures describing regulatory mechanisms of CBF, i.e., the mean flow index (Mx), the cerebral oximetry index (COx) and the modulation index (MI).

Cerebral Autoregulation

Cerebral autoregulation was assessed through the mean flow index (Mx) and cerebral oximetry index (COx).^{30,42} The MAP, CBFV and TSI signal were processed with the use of a moving average filter with a 10 second window, and subsequently the data was resampled to 0.1 Hz, in order to eliminate high-frequency components caused by respiration and pulse waveforms. A continuous, moving Pearson correlation coefficient was calculated over time.

The variables Mx and COx were expressed as the Pearson correlation coefficient between MAP and CBFV and between MAP and TSI, respectively. The Pearson correlation was computed using paired, 10-second averaged values in a five-minute window with three-minute overlap of consecutive windows. This was repeated for the ten-minute windows at the same points as defined earlier. The results were expressed as the median correlation coefficient of these ten-minute window (maximum of five consecutive correlation coefficients).

In this thesis the Mx and COx were calculated according to the following formulas:

$$M_x = \frac{\sum(MAP_i - \overline{MAP})(CBFV_i - \overline{CBFV})}{\sqrt{\sum(MAP_i - \overline{MAP})^2(CBFV_i - \overline{CBFV})^2}} \quad (8)$$

$$CO_x = \frac{\sum(MAP_i - \overline{MAP})(TSI_i - \overline{TSI})}{\sqrt{\sum(MAP_i - \overline{MAP})^2(TSI_i - \overline{TSI})^2}} \quad (9)$$

with $MAP_i, CBFV_i, TSI_i$ as the individual sample points indexed by i and $\overline{MAP}, \overline{CBFV}, \overline{TSI}$ as the window mean.

Neurovascular Coupling

Since NVC generates slow changes in CBFV, only low-frequency content is of importance. The CBFV signal was filtered with the use of a bandpass filter between 0.01 to 0.15 Hz. To be able to make a direct comparison between the CBFV signal and the EEG signal, the CBFV signal was upsampled from 125 Hz to 128 Hz to ensure synchrony. The five EEG bands were extracted through discrete wavelet transform (DWT) in order to calculate the CFC per subband.⁴³ In this study we determined the CFC with the use of the phase-amplitude coupling. For this reason, a Hilbert transform was applied to extract the phase $\varphi(t)$ and amplitude $A(t)$ from the TCD and EEG signal, respectively. The coupling is defined as the modulation index (MI), a quantitative measure recommended for noisier data and shorter epochs.³⁵ The MI was calculated according to the steps described by Tort et al (2010).⁴⁴

The data was divided in two-minute windows over which the phases $\varphi_{TCD}(n)$ were binned and the corresponding average amplitude $A_{EEG}(n)$ over each phase bin was calculated. This was repeated for the length of the signal with a 25% overlap. Afterwards, the mean amplitude per phase bin was determined and normalized. The quantitative MI measure was based on an adaptation of the Kullback-Leibler (KL) distance. This statistic measure is widely used in statistics and describes the difference between two distributions P and Q, defined as

$$D_{KL}(P, Q) = \sum_{j=1}^N P(j) \log \left(\frac{P(j)}{Q(j)} \right) \quad (10)$$

The MI was defined as the KL distance of the observed amplitude distribution (P) from the uniform distribution (U) divided by $\log(N)$:

$$MI = \frac{D_{KL}(P, U)}{\log(N)} \quad (11)$$

with $MI \in [0,1]$.

In the absence of phase-amplitude coupling, the mean amplitude is uniformly distributed over the phases ($P = U$), thus the MI would be 0. When the difference between the observed amplitude distribution (P) and uniform distribution (U) increases, the MI will increase with it.

Intact NVC was defined as a calculated MI statistically different from surrogate control MI's. Surrogate control MI's were calculated with the use of randomly shuffled data windows of both EEG and TCD segments, on the basis that no coupling was assumed to be present in randomly shuffled data. This comparison between the calculated MI and surrogate control MI is especially important when assessing

the MI of a short data epoch. Random fluctuations, caused by noise, can result in artifactual coupling. When the length of the data epoch increases, noise becomes less influential since these random fluctuations are averaged. Statistical significance is determined with the use of a one-tailed non-parametric Whitney-Mann-U test. The results were illustrated as the MI over time. The timeline was divided in 6 segments; during surgery as before ECC, during ECC, after ECC and during ICU admission as <6hr, 6-12hr and >12hr at the ICU. Results were expressed as the mean and standard deviations.

3 RESULTS

3.1 FEASIBILITY

Between May and October of 2022, four patients were included in this study. During this period, a total of 19 patients were screened, from which six patients signed informed consent. The main reason for participant refusal was fear of the placement of the jugular bulb catheter and perceived risks. Due to logistic reasons, e.g., absence of one of the members of the research team, two patients were excluded. From the four included patients, three patients underwent a Bentall procedure and one underwent a SCAR procedure. Only one patient (number 3), developed a delirium during the stay in the hospital. Table 2 illustrates the demographics and clinical data of the included patients. All patients were sedated with the use of propofol and midazolam during surgery.

Table 2: Demographics and clinical data of the included patients. BMI: Body Mass Index in kg/m², PND; post neurological deficits. ECC: extracorporeal circulation.

Patient	Gender	Age (yr)	BMI	PND
1	M	57	25.6	-
2	M	78	26.3	-
3	M	66	24.0	Delirium
4	F	82	29.7	-

Patient	Surgery	Surgery time (min)	ECC time (min)	Aortic occlusion time (min)
1	Bentall	307	162	137
2	Bentall	291	149	125
3	Bentall	307	186	141
4	SCAR	207	70	53

The total data set consisted of 76 hours and 28 minutes. Of this dataset, 52.8% contained quality recordings of all modalities simultaneously. In table 3, the percentage of selected data per patient and recording is presented. The table presents the percentage of the data that was selected as quality total in relation to the total amount of time of the recording.

Table 3: Selected data suitable for data analysis in percentage (%), total time in hours). ICU = Intensive Care Unit.

Patient	Surgery	ICU
1	75.5% (5:36hr)	28.0% (15:43hr)
2	82.2% (5:29hr)	47.6% (15:38hr)
3	59.5% (4:58hr)	45.8% (14:59hr)
4	58.2% (3:03hr)	25.9% (14:02hr)

Based on visual inspection of the data, multiple forms of artefacts in the data were noticed. An example of the synchronized ICM+ dataset with ABP, the CBFV, TSI and spO2 signal is provided in figure 5A. During the period of ECC, the pulsatile behavior of the signals disappeared while slow oscillations were visible (figure 5C). During surgery, electrosurgical instruments were used to coagulate and dissect tissue. The electrical current used for coagulation influenced the signal, especially the TCD signal, resulting in substantial loss of data (figure 5B). As the electric knife was regularly used at the start of the surgery, the amount of useful data was limited during this time. Another cause for loss of data was the moment extubation in the ICU. During the removal of the endotracheal tube from the patient, the head was moved leading to displacement of the TCD cap, with loss of the CBFV signal as a result (figure 5D). A similar problem was encountered at the time that the patient woke up at the ICU (figure 5E), with loss of signal due to excessive movement. Technically, measuring data before start of ECC was challenging, due the anesthetic procedures that occurred at the same time. Furthermore, the EEG signal was also affected due to an artifactual signal originating from the ECC device (see appendix 1 for details).



3.2 CEREBRAL SUPPLY AND DEMAND OF BLOOD AND OXYGEN

Cerebral supply and demand of blood and oxygen was measured over time in four patients. In figure 6, an overview of the results of the four patients is illustrated. First the changes of individual parameters over time will be highlighted, followed by the relationship between specific parameters.

Mean Arterial Pressure

The median MAP remained stable at 64.8 mmHg (IQR 59.8 – 66.6) at induction of anesthesia and 64.5 mmHg (IQR 54.2 – 70.4) during surgery. Thereafter, MAP gradually increased to 73.5 mmHg (IQR 71.8 – 75.3) at admission to the ICU and 89.2 mmHg (IQR 83.1 – 94.6) the next morning after awakening (figure 7A). 06:00am. In general, MAP was lower during surgery compared to the post-operative measurements. The variability between patients increased during surgery.

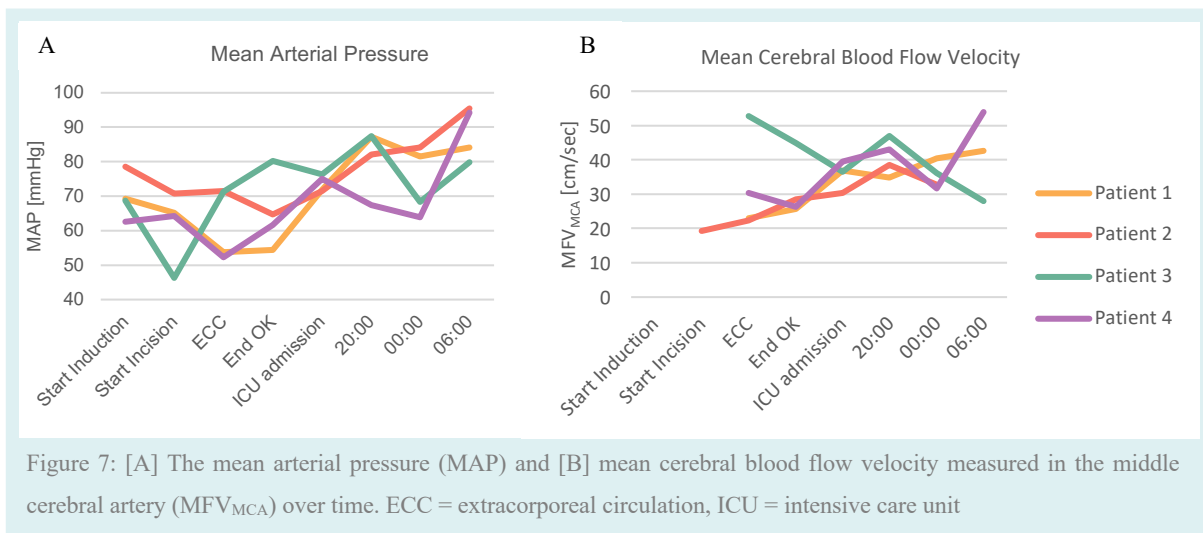


Figure 7: [A] The mean arterial pressure (MAP) and [B] mean cerebral blood flow velocity measured in the middle cerebral artery (MFV_{MCA}) over time. ECC = extracorporeal circulation, ICU = intensive care unit

Mean Cerebral Blood Flow Velocity

In all patients, CBFV signal measured on the right side was used in the analyses of data. In all patients, the MFV_{MCA} generally followed the trend of MAP over time (figure 6). The median MFV_{MCA} over all patients increased from 26.7 cm/s (IQR 22.8 – 35.9) during ECC, to 36.7 cm/sec (IQR 35.0 – 37.5) at ICU admission and 42.6 cm/s (IQR 35.3 – 48.2) measured the next morning at 06:00AM (figure 7B). In patient 1 and 2, the MFV_{MCA} increased in the time between surgery and ICU. In patient 3, the MFV_{MCA} also peaked at 20:00pm but decreased afterwards.

Overview of Cerebral Supply and Demand

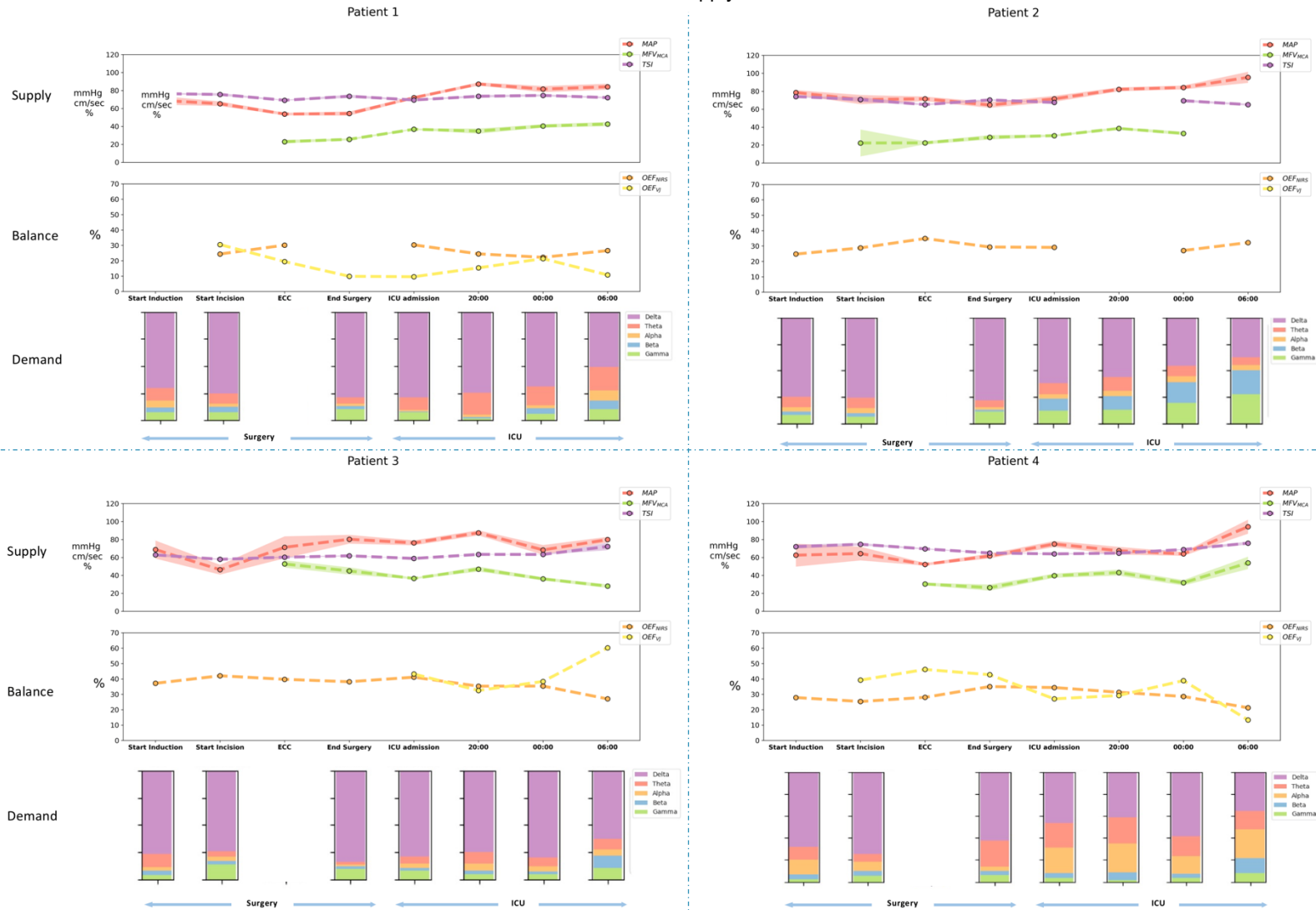
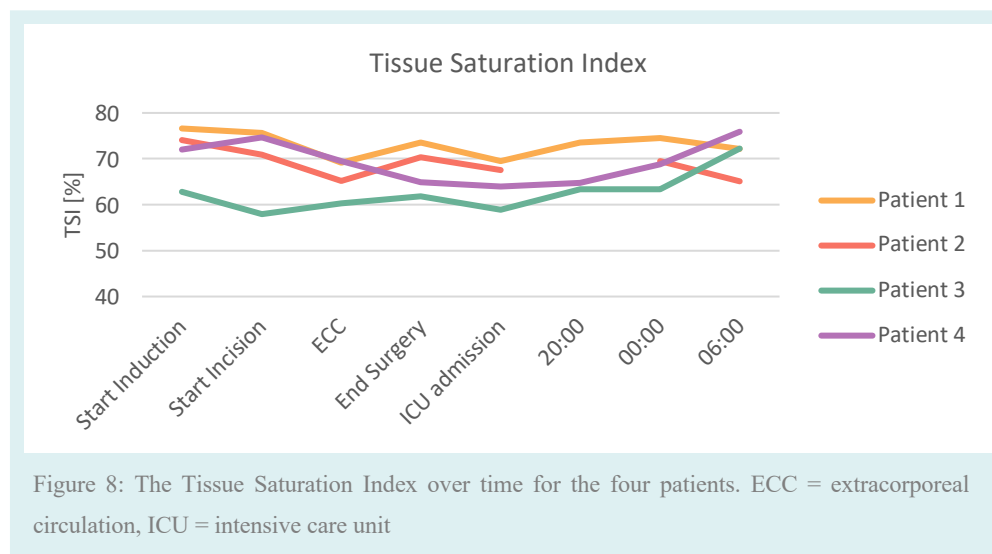


Figure 6: Results of four patients. Each patient-specific plot is divided in a supply, balance and demand graph, with the timepoints on the x-axis. The supply graph shows parameters Mean Arterial Pressure (MAP), Tissue Saturation Index (TSI) and Mean Flow Velocity in the left and/or right Middle Cerebral Artery (MFV_{MCA}). The balance graph portrays the parameters that illustrate the regional and global oxygen extraction measured with NIRS (OEF_{NIRS}) and the jugularis catheter (OEF_{VJ}) respectively. In the demand graph the EEG signal is illustrated as the relative power of the frequency bands. Due to ECC artifacts in the EEG, no reliable calculation of relative frequency power could be made at the ECC timepoint. ICU = Intensive Care Unit, ECC = Extracorporeal circulation.

Tissue Saturation Index

The TSI remained relatively stable in time and was 72.7% (IQR 67.6 - 74.8) at start of incision and 72.2% (IQR 70.3 – 73.1) at 06:00AM the next morning (figure 8). In patient 3, TSI was relatively lower compared to the other three patients, especially during surgery; the median TSI of patient 3 was 61.0% (IQR 59.7 – 62.0) versus the median TSI of other patients 74.6% (IQR 72.5 – 75.8), 70.6% (IQR 69.0 – 71.6) and 70.8% (IQR 68.4 – 72.7) for patient 1, 2 and 4, respectively. Additionally, in patients 1, 2 and 4, the TSI parameter decreased from start of incision to ECC, with a relative decrease of 8.5%, 8.3% and 7.3%, respectively.



Relative EEG power

In all patients the EEG increased in frequency from surgery to the next morning at the ICU. At the ICU, the relative power of the delta band decreased, and higher frequencies emerged towards the measurement at 06:00am (figure 6). In figure 9, an example of the spectrogram of the EEG signal of one patient was provided. In this spectrogram the frequency content of the EEG measurement was illustrated from start of the procedure until the patient awakes at the ICU. The spectrogram shows generalized slowing of EEG during surgery. During surgery lower frequencies were more dominant whereas the power of higher frequencies increases towards the moment of waking up at the ICU.

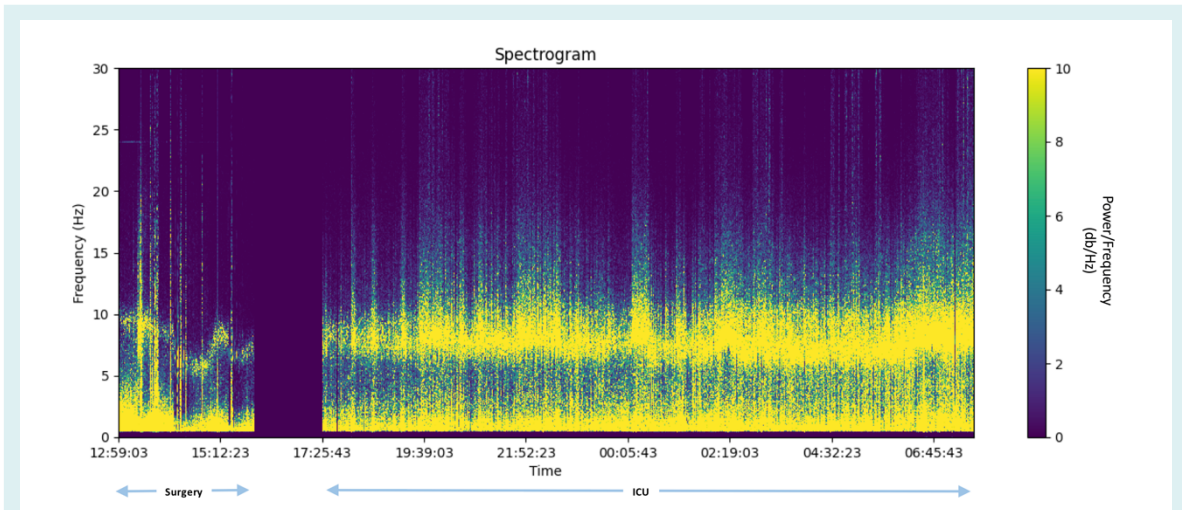


Figure 9: Spectrogram of the EEG signal from the start of surgery until the patient awakes at the ICU. The gap seen at +/- 16:00pm is the stop of recording between the end of surgery and admission at ICU. ICU = Intensive care unit

Oxygen Extraction Fraction

Jugular bulb samples were collected in patient 1, 3 and 4. In patient 2, the jugular bulb catheter could not be placed and in patient 3, the samples collected during surgery were inadequately processed and could not be analyzed. The trend of the global oxygen extraction was different in each patient (figure 10). In patient 1, the oxygen extraction was lower in general compared to the other two patients. Especially the measurement at 06:00am differed, as patient 1 and 4 showed a decrease in oxygen extraction, whereas patient 3 had a sudden increase in oxygen extraction.

In figure 11, the oxygen saturation in arterial, central venous and jugular bulb blood samples was illustrated. The jugularis oxygen saturation in patient 1 remained above 70% at all time points. In figure 11, multiple timepoints illustrated a $S_{vj}O_2$ close or even above the central venous saturation. The brain extracts more oxygen compared to other organs and this should therefore result in lower venous oxygen

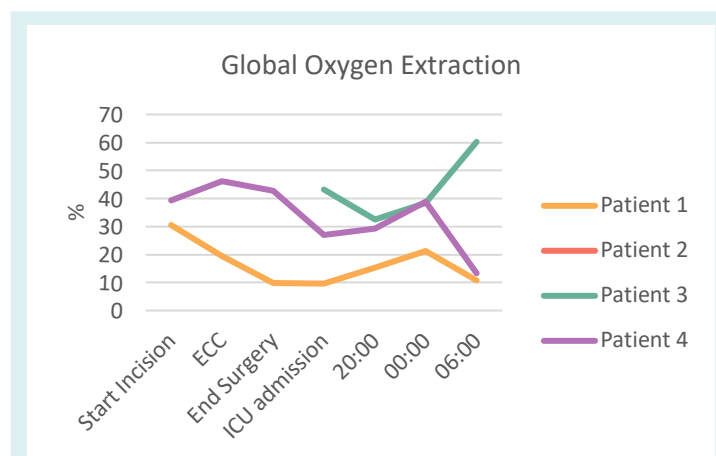


Figure 10: The global oxygen extraction over time. ECC = extracorporeal circulation, ICU = intensive care unit

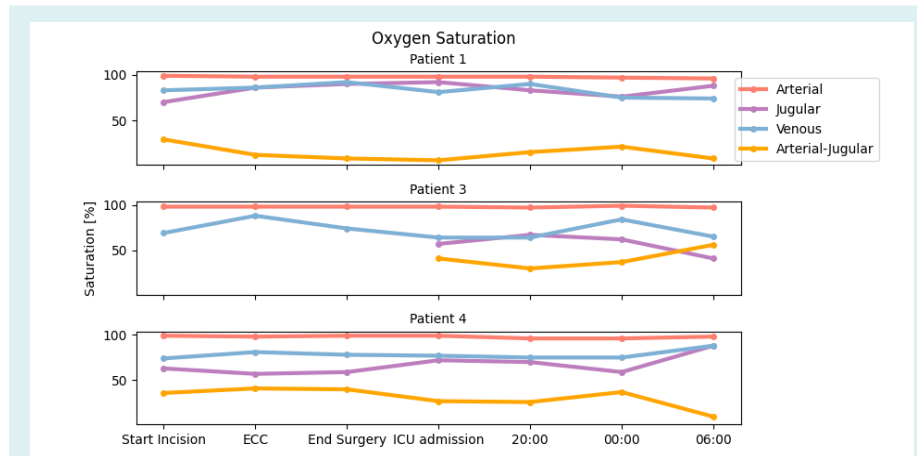


Figure 11: Oxygen saturation over time in patients 1, 3 and 4. The arterial oxygen saturation is shown in red, the jugular saturation in purple, central venous saturation in blue and the difference between arterial and jugular in orange. ECC = extracorporeal circulation, ICU = intensive care unit

saturation. It is known that an aspiration rate of > 2 ml/min can lead to considerable contamination of extracranial blood.⁴⁶ For this reason, we discarded all values above 80% on the basis of presumably contaminated samples, given there was no clinical context explaining these values.

The regional oxygen extraction, measured with NIRS, found a median OE_{NIRS} of 28.7% (IQR 26.1 – 34.5) and remained stable over time. We compared regional O_2 extraction measurements (via NIRS) to global measurements based on jugular bulb samples. The regional oxygen extraction parameter fluctuated less compared to the global oxygen extraction and did not follow the same trend (figure 6). The correlation between the global oxygen extraction measured with the jugularis catheter and the regional oxygen extraction measured with NIRS is shown in figure 12. This figure illustrates a poor correlation between the remaining global and regional oxygen extraction measurements with a Pearson correlation coefficient of 0.13.

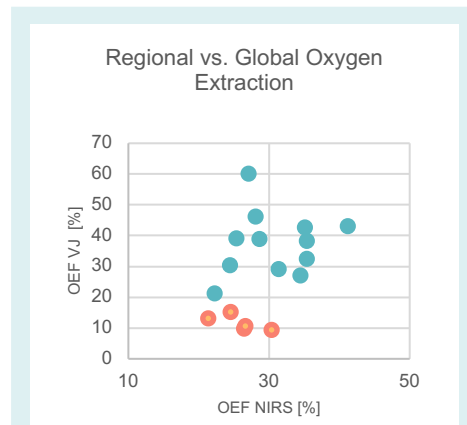


Figure 12: A scatterplot illustrating the relation between global and regional oxygen extraction measured with the jugularis bulb catheter (OE_{VJ}) and NIRS (OE_{NIRS}), respectively. The rejected measurements based on erroneous sample collection (figure 10) are illustrated in orange.

3.3 REGULATORY MECHANISMS OF CEREBRAL BLOOD FLOW

Cerebral Autoregulation

The presence of cerebral autoregulation was evaluated with the use of the Mx and COx using a threshold of 0.45 to indicate active or passive autoregulation.

Mean Flow index (Mx)

The Mx was below the threshold for passive autoregulation at all time points for all patients, except for the Mx measurement of patient 4 at 06:00am (figure 13). This suggests that, apart from this measurement, cerebral autoregulation was intact during the complete time period for all patients. The trend in Mx differed considerably over time and between patients.

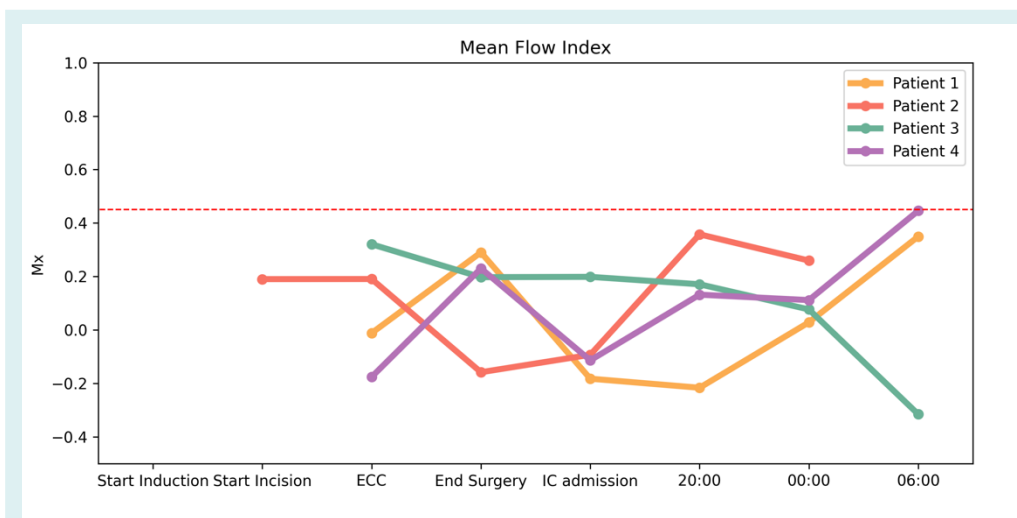


Figure 13: The mean flow index (Mx) over time in all patients. The red dashed line illustrates the threshold (0.45) above which cerebral autoregulation is impaired.

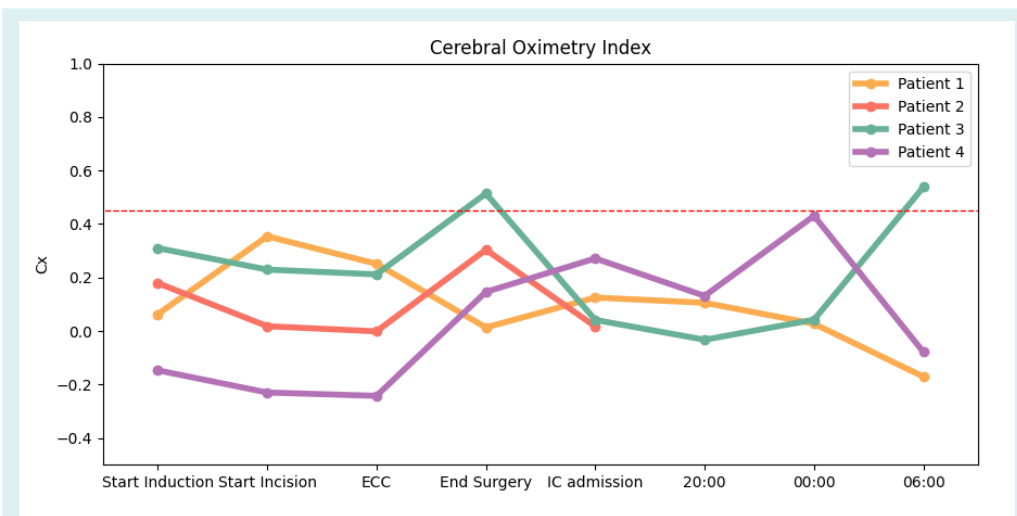


Figure 14: The cerebral oximetry index (COx) over time in all patients. The red dashed line illustrates the threshold (0.45) above which cerebral autoregulation is impaired.

Cerebral Oximetry Index (COx)

All COx values were below the threshold for passive autoregulation, except for patient 3 at the end of surgery and the 06:00am (figure 14). Additionally, the trend in COx also differed considerably over time and between patients.

Neurovascular Coupling

Figure 15 shows the average MI index for all four patients, describing the CFC coupling between the EEG and CBFV signal. During ECC, the MI could not be calculated due to artifactual signal originating from the ECC device in the EEG signal. The MI was only significantly different from the surrogate control MI at ICU < 6hr stay, highlighted in yellow, suggesting that NVC was absent at most timepoints except the ICU < 6hr segment. In figure 16 the MI was provided per frequency band. In general, the MI indices of all frequency bands decreased over time, except for the delta band. Before ECC, all frequency bands except for the delta band, showed significant MI values. After ECC, the alpha, beta and gamma band still showed significant MI values, whereas the theta band was the only band with significant MI values during the first six hours at ICU. This suggest there is NVC in the higher frequencies during surgery and in the lower frequencies during ICU. No differences between the MI calculated per EEG reference were found (data not shown).

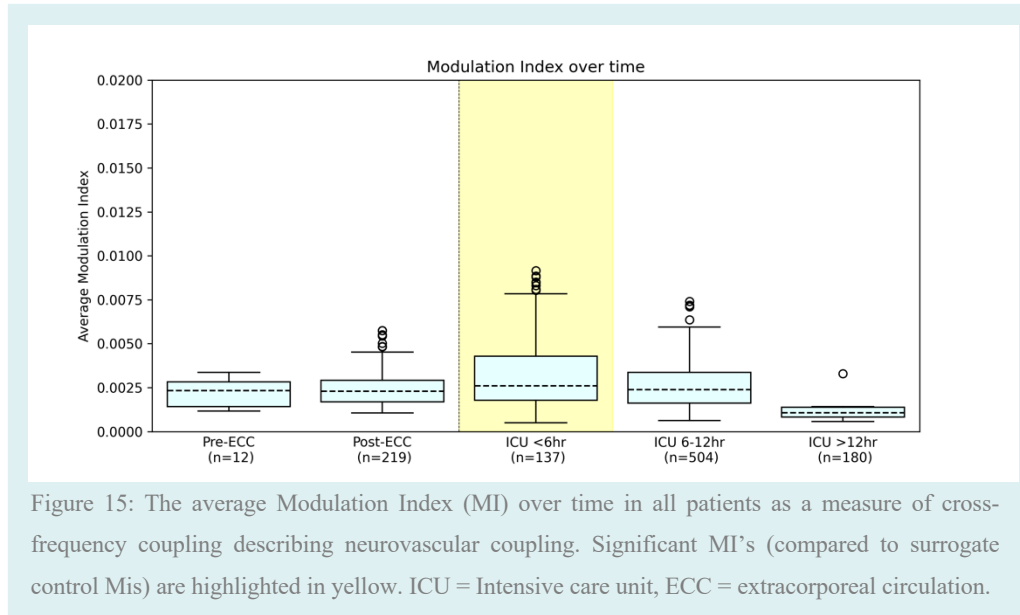
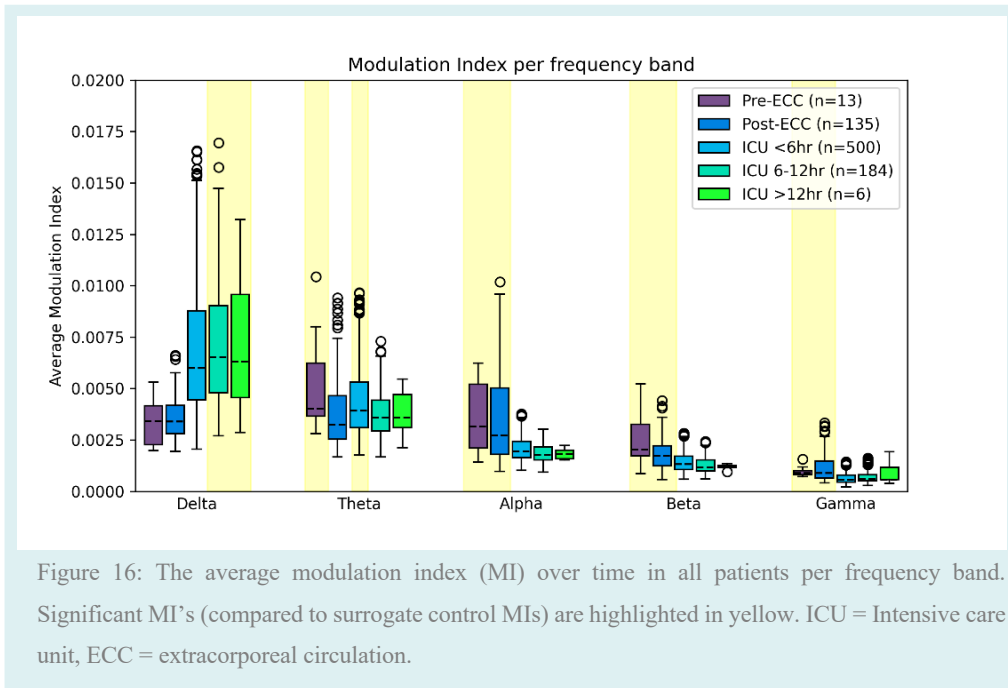


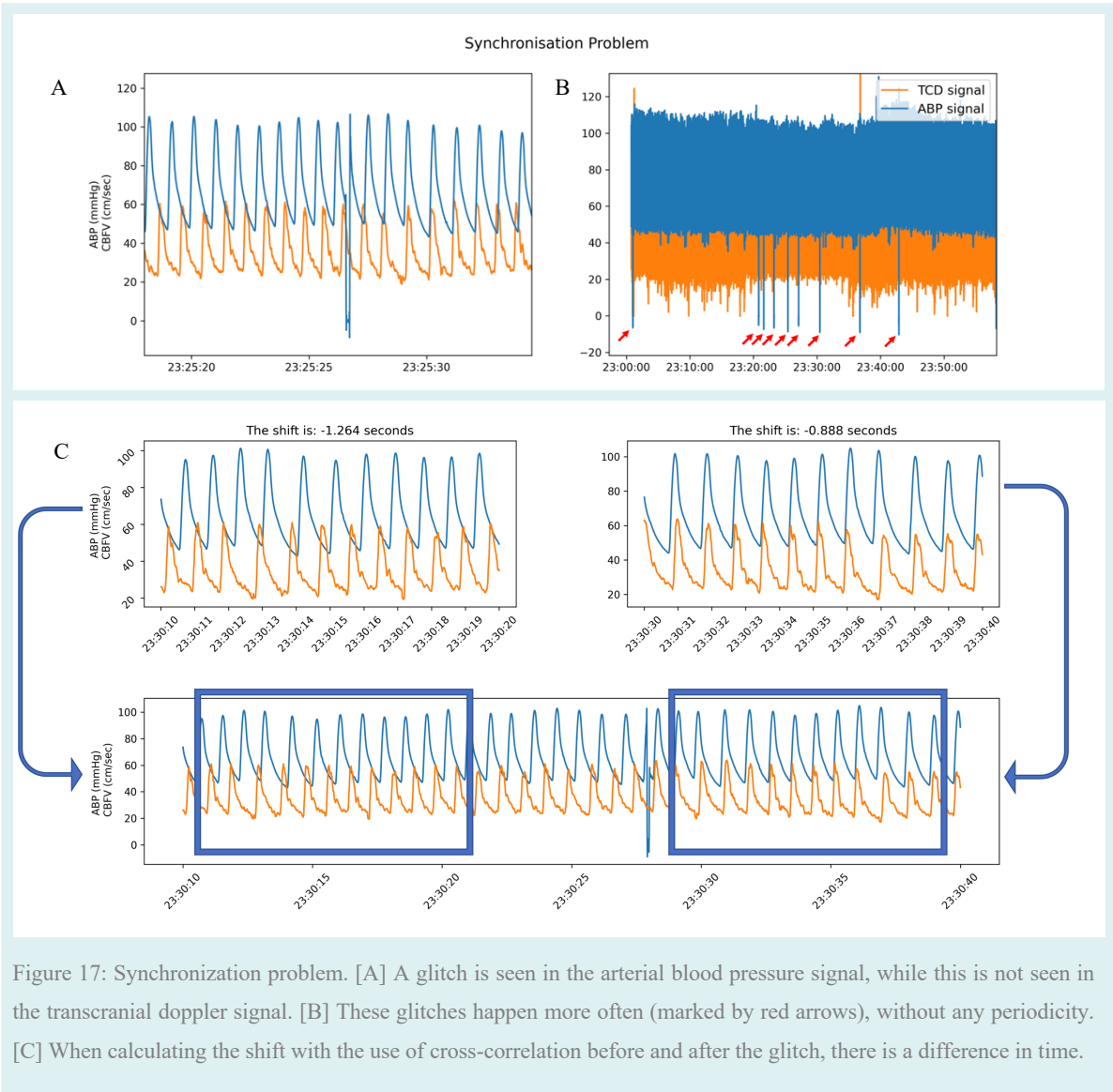
Figure 15: The average Modulation Index (MI) over time in all patients as a measure of cross-frequency coupling describing neurovascular coupling. Significant MI's (compared to surrogate control Mis) are highlighted in yellow. ICU = Intensive care unit, ECC = extracorporeal circulation.



3.4 SYNCHRONIZATION PROBLEM

Data was imported into ICM+ to warrant synchronization, however, this works insufficiently. ICM+ imported the TCD, NIRS and monitor data. Whereas the TCD and NIRS data ran synchronously, the monitor data was seen with a delay. The problem was detected through aberrant heartbeats, which were seen at different timepoints in the monitor data compared to the remaining ICM+ data.

In figure 17, the ABP signal and TCD signal are plotted. It can be seen that the ABP signal (in blue) glitches, seen as a sudden drop to zero, and restarted immediately after. However, the restart was not how one would expect the signal to continue, mainly because there was no change in the TCD signal. These glitches were found throughout the complete dataset and did not seem to follow periodic behavior. Figure 17b illustrates an hour of data with multiple glitches (marked with the red arrows). By performing cross correlation per segment, the delay could be identified through comparing the frequency content of the data. Unfortunately, when performing this technique within one segment before and after a glitch, the resulting delay was not constant, see figure 17c. This suggested that the delay is dynamic and cannot be eliminated easily.



4 DISCUSSION

In this thesis we studied the balance between cerebral supply and demand during aortic arch surgery until the moment of awakening with extensive multi-modal monitoring. We demonstrate that parallel neuromonitoring with TCD, NIRS, EEG and jugular venous oximetry was feasible and accommodated evaluation of various quantitative measures describing cerebral hemodynamic regulatory mechanisms.

4.1 FEASIBILITY OF THE STUDY

The primary outcome parameter of this part of the study was its feasibility. The set-up of this study is complex and requires the cooperation of multiple departments. To date, most studies have investigated the relationship between post neurological complications and one or two diagnostic techniques. To our knowledge we were the first to investigate cerebral perfusion with a multimodal monitoring set-up of this extent. In this study, we demonstrated that multimodal monitoring with these techniques was feasible and provided us with both temporal information of the multiple processes influencing cerebral perfusion and their interactions. Another main advantage of the multimodal neuromonitoring used in this study, was the ability to measure both globally and regionally while focusing on multiple mechanisms simultaneously. Currently, there is no true golden standard for neuromonitoring as all techniques have their strengths and limitations. Literature suggests that the interplay between the physiological processes influencing cerebral oxygenation and hemodynamics is too complex for a single modality.^{63,64} Hence, we believe that the strength of our study lies in the multimodal approach. Combining the use of individual neuromonitoring techniques will help reduce the limitations and will provide more patient safety during cardiac surgery.⁶⁵ The multimodal approach increases the chance of identifying cerebral perfusion problems, as illustrated in the case report of a perioperative stroke during carotid endarterectomy described by Michels et al (2022).⁶⁶

Through the first measurements, we encountered several challenges that provided us with learning points for future measurements. One of the main challenges was to find a TCD signal of good quality. Finding the right position of the TCD probe to record a good quality signal can be difficult and can take time. The goal was to obtain the signal before the start of the procedure, however in order to adjust the TCD probe, the researcher needed to stand at the head of the bed, while this was also the territory of the anesthesiologist. Induction and the start of the procedure was an important moment for the anesthesiologist, resulting in limited space and time for the researcher to adjust the TCD probe and find the correct angle. The result was that often we would only get a good quality TCD signal between 30-60 minutes after the start of the procedure. Another focus point was the method of aspiration of blood samples from the jugular bulb catheter. This catheter is not used in daily clinical practice, which means that most nurses and doctors were unfamiliar with this system. We measured oxygen concentrations in jugular blood samples that were presumably the result of incorrect aspiration, as rapid aspiration results

in contamination of the sample with extracerebral blood. Lastly, the instruments involved during ECC, influenced the EEG signal during surgery. We did not succeed in eliminating this artifactual signal without distorting the EEG signal of interest, which influenced the calculation of the relative frequency bands and the MI.

4.2 RESULT INTERPRETATION

Cerebral supply and demand parameters

Based on the results of the four patients included in our study, we found that cerebral demand measured with EEG and cerebral supply measured as MFV and MAP increases from surgery towards the moment of awakening at the ICU. We did find a high interpatient variability in the parameters over time, making general interpretation of the results complex. This high variability could have been influenced by multiple factors, e.g., heterogeneity of the study population, measurement errors or synchronization problems.

Power in the higher frequency bands increased in all patients towards the moment of awakening at the ICU. This is in line with literature, as the emergence from general anesthesia is characterized by a loss in power in the slower delta frequency bands, and a recovery of power in the higher frequency bands.⁴⁷ This indicates that, as expected, the cerebral demand increases in the period from deep anesthesia during surgery towards the moment of awakening at the ICU. Along with this increase in cerebral demand, we measured an increase in MFV. This indicates that the increase in cerebral demand was accompanied by an increase in cerebral supply.

Remarkably, the MFV measured in this study (median of 35.4 cm/sec) is lower compared to the normal range of 49.6 - 56.6 cm/s.³⁸ The TCD signal requires technical skill, is operator dependent because of the dependency of the insonation angle and is known for its long learning curve.^{51,52} In our study we used a so-called 'pure doppler' probe, which means that only the velocity signal is recorded without additional visual information. For this reason, signal quality could be influenced by unnoticed probe dislocation causing measurement in the posterior cerebral artery, known for its lower MFV. Besides, the TCD signal was prone to artifacts, especially caused by movement. In patient 2, no TCD measurement was possible at 06:00am due to agitation at the time of waking up.

Cerebral oxygenation decreased from start of incision to the moment of ECC in three patients. This decrease in TSI can be multifactorial; it could be the result of hypoperfusion or relative hypoxemia.⁴⁹ We measured peripheral saturation simultaneously and did not find arguments for hypoxemia. Higami et al., found that a decline to 70% of baseline saturation was significant for ischemic events.⁵⁰ This leads

us to believe that a decline of 8 percent is not likely to have caused neurological complications, but may be interpreted as a consequence of a decrease of cerebral demand.

Global oxygen extraction differed over time in patients. The normal range for $S_{vj}O_2$ is between 55% and 75%, in which a value below 55% indicates desaturation and a value above 75% indicates hyperemia or low cerebral oxygen consumption.⁵³ In a critical situation, a high $S_{vj}O_2$ is seen when the brain is unable to extract oxygen due to neuronal cell death or when cerebral pressure is too high, leading to shunting of arterial blood to the venous system. The high values found in our study may have been caused by measurement errors rather than physiological mechanisms. This argument is strengthened by the proximity of the $S_{vj}O_2$ to the central venous oxygen saturation. As the brain's oxygen extraction is higher compared to other organs, central venous oxygen saturation should be higher. It is known that the $S_{vj}O_2$ can be strongly affected by misplacement of the catheter or an aspiration rate $>2\text{ml/min}$. This can lead to contamination from extracranial vessels and therefore falsely high $S_{vj}O_2$ leading to false interpretation.²⁷

In our results we found a low correlation between regional and global oxygen extraction and saturation. Reviewing literature, stronger correlations were described, such as the study by Naguib et al (2017) who found a correlation of 0.78 between regional and global oxygen saturation in children undergoing cardiac operations.⁵⁴ We realize that before we can truly draw a conclusion from the relation between regional and global oxygen extraction, we need more data. Even though the number of measurements included for this correlation was an important limiting factor, there are additional possible explanations for the low correlation. The regional oxygen extraction is calculated with the TSI parameter which only reflects oxygen saturation in the anterior circulation of the prefrontal cortex, limiting the monitoring ability to an area of approximately 1cm^2 .^{55,56} While on the other hand, global oxygen extraction is a heterogeneous measure, meaning anatomic variations can lead to unpredictable contamination and might miss focal hypoxia.¹³

We examined the cerebral autoregulation as the relationship between MAP and CBFV through the mean flow index (Mx) and the relationship between MAP and TSI through the cerebral oximetry index (COx). We found a strong variation in both Mx and COx over time. In general, Mx and COx suggested intact autoregulation for most patients at most time points. Occasionally, Mx and COx suggested impaired autoregulation. Remarkably, signs of impaired autoregulation occurred inconsistently and with disagreement between Mx and COx. However, we realize these findings are highly preliminary as they are based on a cohort of four patients. In contrast to our findings, Brady et al. (2010) found a significant correlation of 0.55 between the Mx and COx, while a loss of autoregulation resulted in a larger Mx compared to COx.³⁰ The difference with our study might have resulted from the limited number of windows used in our method, as we only evaluated the correlation at specific timepoints. Additionally, problems in synchronization might have influenced our results. The correlation was calculated over 30

samples which each represent a ten-seconds mean of the respective signals. Although we believed that the synchronization problem was of minimal influence, these results raise suspicion. In this study a threshold above 0.45 was used to define impaired cerebral autoregulation.³⁰ The correct threshold remains a topic of discussion, as studies have also reported impaired cerebral autoregulation by using a threshold of 0.3.⁵⁷ Instead of evaluating the presence of cerebral autoregulation by a fixed threshold, patient specific limits of autoregulation would be more clinically relevant.

In this thesis we calculated a novel metric for NVC monitoring during aortic arch surgery, the MI. This metric was derived from the work by Liu et al, who calculated the MI for patients with stroke. By using this metric, our results suggested that none of the patients had neurovascular coupling. Nonetheless all patients in our study woke up without presenting signs of major neurovascular problems. The work by Liu et al, is the only prior work describing the MI as a metric for NVC. In their study (n=16) they found a difference between the MI in the deceased group and survival group of patients with stroke, though not significantly. Beside the fact that our study population differs from the study population in Liu's study, there are also differences in methods that need to be considered. We computed the mean MI instead of the sum of all, in order to test for statistically significant NVC. Furthermore, during aortic arch surgery, multiple sedatives were administered at high dose of which the effect on neurovascular coupling are unknown.⁵⁹ To conclude, we were not able to validate this new metric and advice further analysis of this metric in a larger cohort before conclusions can be drawn. Additionally, this method describes a regional NVC with rather global parameters as CBFV and EEG activity. As NVC is mainly a local mechanism, it could be interesting to investigate the MI between NIRS signals and local EEG.

Post neurological deficits

The eventual goal of this study is to determine whether a change in cerebral perfusion during aortic arch surgery is linked to the development of post neurological deficits, such as delirium. In this thesis, only one patient developed a delirium while admitted to the cardiac-thoracic ward, with a maximum ICDSC score of 5. While acknowledging that n = 1 is too small to draw any conclusions, we do want to reflect on our findings as we see several elements worth highlighting. First of all, the median TSI in this patient was lower than the other 3 patients (62.3% versus 73.6%, 69.5% and 69.2%). Studies have demonstrated that low cerebral oxygen saturation is an independent risk factor for the development of delirium in critically ill patients.^{60,61} However, the systematic review of Zheng et al (2013) concluded that the specificity of solely regional saturation monitoring for PNDs could not be established, as the absence of reductions in regional saturation were no guarantee for adequate cerebral blood flow.⁶² Another distinct difference between the patient with delirium and the other patients, was the sudden decrease in $S_{vj}O_2$ during awakening. As the cerebral demand did increase, supported by the shift in EEG frequencies, the cerebral supply parameters only increased slightly. This might have been an indication of a mismatch in cerebral supply and demand.

4.3 LIMITATIONS & RECOMMENDATIONS

The main limitation of this thesis was the size of the study population. Due to the small sample size, the confidence interval is large as it remains unclear whether the variation seen in the results is indeed caused by a mismatch between cerebral supply and demand or not. It is yet unknown whether the results of these patients are representative of the patient group or whether they illustrate exceptions to the rule. Besides the fact that sample size is small, the patients underwent different surgical procedures and were in different age groups. It is known that both transcranial doppler measurements and EEG signals are affected by age.³⁸ The relevance of our findings on clinical outcome remain to be investigated. A similar research with a larger sample size can provide more information on the relationship between cerebral supply and demand parameters. In addition, we chose to visualize and analyze our data at specific timepoints to obtain an overview of all the parameters. Many of the results in our study illustrate the average behavior of the parameter within a 10-minute segment. Future research will benefit from more detailed evaluation of the parameters over time as possible influential events might be missed.

Secondly, an important limitation in the ICM+ dataset was the deficiency of synchronization between the monitor data and the other data such as the TCD and NIRS signal. All data from the monitor was directly imported with the use of an RS232 cable, but it appeared that the monitor data was imported with a delay, as explained in the results. Due to this delay, the data was not synchronized to the second as expected. Since we calculated our results with the use of a ten-minute mean, the influence of this delay was assumed minimal in this thesis. However, the results of this study should still be interpreted with caution. Furthermore, this issue precluded calculations of dynamic cerebral autoregulation in the frequency domain, such as transfer function analysis. Currently, we have consulted the manufacturer of the ICM+ program, to address this problem for future measurements. In this study, we examined cerebral autoregulation through the use of MAP, TSI and CBFV signals. Recently Elting and colleagues developed the so-called ‘Transit Time – Blood Flow /Blood volume (TT-BF/BV) model’ of cerebral circulation in which the O₂Hb concentration represents the ABP, and the HHb concentration represents the CBFV.⁶⁷ In this model it is assumed that oscillations in O₂Hb concentration arise mainly from the arterial compartment, whereas the oscillations in HHb concentration are mostly seen in the venous compartments. For this reason, the relationship between these two provides a proxy of cerebral autoregulation. As both parameters are recorded within the same device, this measure will not be affected by any synchronization problems. In future research it could be valuable to investigate the results of cerebral autoregulation with this technique.

Thirdly, the EEG signal was affected by an artifactual signal from the ECC device during surgery. The artifactual signal caused by the ECC, could not be eliminated with a bandpass filter without distorting the EEG signal that we were interested in. We did not succeed in eliminating this signal with the use of an adaptive filter or independent component analysis. For future purposes, this should be further

investigated. The remaining artifactual signal inhibited us from performing direct reliable comparison calculation between the EEG signal and other parameters during the ECC time.

Fourthly, the TCD signal contained a large variety of artifacts, all influencing the signal quality. While the manual selection of data and automatic artifact detection algorithm handled most artifacts, the signal was still affected by occasional artifacts. The artifacts shorter than 3 seconds in the data were filled with the use of linear interpolation. In this study we opted for this relatively simple technique since we only evaluate the mean signal. When data is used for future research, this step in the data analysis should be revisited.

Lastly, we did not adjust for multiple comparisons. As mentioned before, the regulation of cerebral hemodynamic is complex and changes in CBF are multifactorial. Furthermore, we did not record data from the ECC-machine. The machine collects continuous data including blood temperature, flow and saturation. To be able to correct for changes that are caused by the ECC device, this data will be useful. For future measurements, the additional recording of ECC parameters should be considered.

5 CONCLUSION

In this pilot-study we examined feasibility of perioperative multimodal monitoring and studied the balance between cerebral supply and demand. With the setup of this study, the cerebral perfusion can be monitored throughout the complete admission of patients undergoing aortic arch surgery and different cerebral hemodynamic mechanisms can be evaluated simultaneously. In the results, we demonstrated a high interpatient variability. Future research will benefit from technical improvements of the measurement set-up, advancements in the signal processing focused on synchronicity and a larger study population.

6 REFERENCES

1. Qu, J. Z. *et al.* Brain Protection in Aortic Arch Surgery: An Evolving Field. *J. Cardiothorac. Vasc. Anesth.* **35**, 1176–1188 (2021).
2. Pierri, M. D., Capestro, F., Zingaro, C. & Torracca, L. The changing face of cardiac surgery patients: an insight into a Mediterranean region. *Eur. J. Cardio-Thoracic Surg.* **38**, 407–413 (2010).
3. Brown, J. M. *et al.* Isolated aortic valve replacement in North America comprising 108,687 patients in 10 years: Changes in risks, valve types, and outcomes in the Society of Thoracic Surgeons National Database. *J. Thorac. Cardiovasc. Surg.* **137**, 82–90 (2009).
4. Hood, R., Budd, A., Sorond, F. A. & Hogue, C. W. Peri-operative neurological complications. *Anaesthesia* **73**, 67–75 (2018).
5. Centofanti, P. *et al.* Neurologic and cognitive outcomes after aortic arch operation with hypothermic circulatory arrest. *Surgery* **160**, 796–804 (2016).
6. Liu, J. *et al.* Incidence, Predictors and Outcomes of Delirium in Complicated Type B Aortic Dissection Patients After Thoracic Endovascular Aortic Repair. *Clin. Interv. Aging* **Volume 16**, 1581–1589 (2021).
7. Ely, E. W. Delirium as a Predictor of Mortality in Mechanically Ventilated Patients in the Intensive Care Unit. *JAMA* **291**, 1753 (2004).
8. Tian, D. H., Croce, B. & Hardikar, A. Aortic arch surgery. *Ann. Cardiothorac. Surg.* **2**, 245 (2013).
9. Carrascal, Y. & Guerrero, A. L. Neurological Damage Related to Cardiac Surgery. *Neurologist* **16**, 152–164 (2010).
10. Davies, D. J. *et al.* The Valsalva maneuver: an indispensable physiological tool to differentiate intra versus extracranial near-infrared signal. *Biomed. Opt. Express* **11**, 1712 (2020).
11. Payne, S. *Cerebral Autoregulation. Springer Briefs in Bioengineering* (Springer, 2016). doi:10.1093/nq/s7-IV.95.328-b
12. Bor-Seng-Shu, E. *et al.* Cerebral hemodynamics: Concepts of clinical importance. *Arq. Neuropsiquiatr.* **70**, 357–365 (2012).
13. Milne, B., Gilbey, T., Gautel, L. & Kunst, G. Neuromonitoring and Neurocognitive Outcomes in Cardiac Surgery: A Narrative Review. *J. Cardiothorac. Vasc. Anesth.* **36**, 2098–2113 (2022).
14. Tymko, M. M., Ainslie, P. N. & Smith, K. J. Evaluating the methods used for measuring cerebral blood flow at rest and during exercise in humans. *Eur. J. Appl. Physiol.* **118**, 1527–1538 (2018).
15. Coverdale, N. S., Gati, J. S., Opalevych, O., Perrotta, A. & Shoemaker, J. K. Cerebral blood flow velocity underestimates cerebral blood flow during modest hypercapnia and hypocapnia. *J. Appl. Physiol.* **117**, 1090–1096 (2014).
16. Purkayastha, S. & Sorond, F. Transcranial Doppler Ultrasound: Technique and Application. *Semin. Neurol.* **32**, 411–420 (2013).
17. Claassen, J. A. *et al.* Transfer function analysis of dynamic cerebral autoregulation: A white paper from the International Cerebral Autoregulation Research Network. *J. Cereb. Blood Flow Metab.* **36**, 665–680 (2015).
18. Ter Horst, H. J., Verhagen, E. A., Keating, P. & Bos, A. F. The relationship between electrocerebral activity and cerebral fractional tissue oxygen extraction in preterm infants. *Pediatr. Res.* **70**, 384–388 (2011).
19. Naulaers, G. *et al.* Use of tissue oxygenation index and fractional tissue oxygen extraction as non-invasive parameters for cerebral oxygenation: A validation study in piglets. *Neonatology* **92**, 120–126 (2007).

20. Purdon, P. L., Sampson, A., Pavone, K. J. & Brown, E. N. Clinical Electroencephalography for Anesthesiologists: Part I: Background and Basic Signatures. *Anesthesiology* **123**, 937–60 (2015).
21. Finnigan, S. & van Putten, M. J. A. M. EEG in ischaemic stroke: Quantitative EEG can uniquely inform (sub-)acute prognoses and clinical management. *Clin. Neurophysiol.* **124**, 10–19 (2013).
22. Scheeren, T. W. L., Kuizenga, M. H., Maurer, H., Struys, M. M. R. F. & Heringlake, M. Electroencephalography and brain oxygenation monitoring in the perioperative period. *Anesth. Analg.* **128**, 265–277 (2019).
23. Jordan, K. G. Emergency EEG and continuous EEG monitoring in acute ischemic stroke. *J. Clin. Neurophysiol.* **21**, 341–352 (2004).
24. Hofmeijer, J. & van Putten, M. J. A. M. Ischemic Cerebral Damage. *Stroke* **43**, 607–615 (2012).
25. Hofmeijer, J. & van Putten, M. J. A. M. EEG in postanoxic coma: Prognostic and diagnostic value. *Clin. Neurophysiol.* **127**, 2047–2055 (2016).
26. Murphy, M. *et al.* Propofol Anesthesia and Sleep: A High-Density EEG Study. *Sleep* **34**, 283–291 (2011).
27. Bhardwaj, A., Bhagat, H. & Grover, V. Jugular venous oximetry. *J. Neuroanaesth. Crit. Care* **02**, 225–231 (2015).
28. Mayberg, T. S. & Lam, A. M. Jugular bulb oximetry for the monitoring of cerebral blood flow and metabolism. *Neurosurg. Clin. N. Am.* **7**, 755–65 (1996).
29. Claassen, J. A. H. R., Thijssen, D. H. J., Panerai, R. B. & Faraci, F. M. Regulation of Cerebral Blood Flow in Humans: Physiology and Clinical Implications of Autoregulation. *Physiol. Rev.* (2021). doi:10.1152/physrev.00022.2020
30. Brady, K. *et al.* Real-Time Continuous Monitoring of Cerebral Blood Flow Autoregulation Using Near-Infrared Spectroscopy in Patients Undergoing Cardiopulmonary Bypass. *Stroke* **41**, 1951–1956 (2010).
31. Hendriks, D. *et al.* Measurement of Neurovascular Coupling in Neonates. *Front. Physiol.* **10**, (2019).
32. Phillips, A. A., Chan, F. H., Zheng, M. M. Z., Krassioukov, A. V & Ainslie, P. N. Neurovascular coupling in humans: Physiology, methodological advances and clinical implications. *J. Cereb. Blood Flow Metab.* **36**, 647–664 (2016).
33. Vestergaard, M. B., Frederiksen, J. L., Larsson, H. B. W. & Cramer, S. P. Cerebrovascular Reactivity and Neurovascular Coupling in Multiple Sclerosis—A Systematic Review. *Front. Neurol.* **13**, (2022).
34. Liu, X. *et al.* Cross-Frequency Coupling Between Cerebral Blood Flow Velocity and EEG in Ischemic Stroke Patients With Large Vessel Occlusion. *Front. Neurol.* **10**, (2019).
35. Hülsemann, M. J., Naumann, E. & Rasch, B. Quantification of Phase-Amplitude Coupling in Neuronal Oscillations: Comparison of Phase-Locking Value, Mean Vector Length, Modulation Index, and Generalized-Linear-Modeling-Cross-Frequency-Coupling. *Front. Neurosci.* **13**, (2019).
36. Stouten, S. CEREBRAL PERFUSION DISORDERS IN AORTIC ARCH SURGERY A MULTIMODAL APPROAC. (University of Twente).
37. Krewulak, K. D., Rosgen, B. K., Ely, E. W., Stelfox, H. T. & Fiest, K. M. The CAM-ICU-7 and ICDSC as measures of delirium severity in critically ill adult patients. *PLoS One* **15**, e0242378 (2020).
38. Tegeler, C. H. *et al.* Transcranial Doppler Velocities in a Large, Healthy Population. *J. Neuroimaging* **23**, 466–472 (2013).
39. D'Andrea, A. *et al.* Transcranial Doppler ultrasonography: From methodology to major clinical applications. *World J. Cardiol.* **8**, 383 (2016).
40. Virtanen, P. *et al.* SciPy 1.0: fundamental algorithms for scientific computing in Python. *Nat. Methods* **17**, 261–272 (2020).

41. Correa, A. G., Laciari, E., Patiño, H. D. & Valentinuzzi, M. E. Artifact removal from EEG signals using adaptive filters in cascade. *J. Phys. Conf. Ser.* **90**, 012081 (2007).
42. Ono, M. *et al.* Risks for impaired cerebral autoregulation during cardiopulmonary bypass and postoperative stroke. *Br. J. Anaesth.* **109**, 391–398 (2012).
43. Jacob, J. E., Nair, G. K., Iype, T. & Cherian, A. Diagnosis of Encephalopathy Based on Energies of EEG Subbands Using Discrete Wavelet Transform and Support Vector Machine. *Neurol. Res. Int.* **2018**, 1–9 (2018).
44. Tort, A. B. L., Komorowski, R., Eichenbaum, H. & Kopell, N. Measuring Phase-Amplitude Coupling Between Neuronal Oscillations of Different Frequencies. *J. Neurophysiol.* **104**, 1195–1210 (2010).
45. Newman, L., Nolan, H., Carey, D., Reilly, R. B. & Kenny, R. A. Age and sex differences in frontal lobe cerebral oxygenation in older adults—Normative values using novel, scalable technology: Findings from the Irish Longitudinal Study on Ageing (TILDA). *Arch. Gerontol. Geriatr.* **87**, 103988 (2020).
46. Matta, B. F. & Lam, A. M. The Rate of Blood Withdrawal Affects the Accuracy of Jugular Venous Bulb. *Anesthesiology* **86**, 806–808 (1997).
47. Dressler, O., Schneider, G., Stockmanns, G. & Kochs, E. F. Awareness and the EEG power spectrum: analysis of frequencies. *Br. J. Anaesth.* **93**, 806–809 (2004).
48. Kassam, S. I., Lu, C., Buckley, N. & Lee, R. M. K. W. The Mechanisms of Propofol-Induced Vascular Relaxation and Modulation by Perivascular Adipose Tissue and Endothelium. *Anesth. Analg.* **112**, 1339–1345 (2011).
49. Bevan, P. J. W. Should Cerebral Near-infrared Spectroscopy be Standard of Care in Adult Cardiac Surgery? *Hear. Lung Circ.* **24**, 544–550 (2015).
50. Higami, T. *et al.* Retrograde cerebral perfusion versus selective cerebral perfusion as evaluated by cerebral oxygen saturation during aortic arch reconstruction. *Ann. Thorac. Surg.* **67**, 1091–1096 (1999).
51. Schramm, P. *et al.* Impaired cerebrovascular autoregulation in patients with severe sepsis and sepsis-associated delirium. *Crit. Care* **16**, R181 (2012).
52. Naqvi, J., Yap, K. H., Ahmad, G. & Ghosh, J. Transcranial Doppler Ultrasound: A Review of the Physical Principles and Major Applications in Critical Care. *Int. J. Vasc. Med.* **2013**, 1–13 (2013).
53. Senapathi, T. G. A. *et al.* Jugular bulb oxygen saturation correlates with Full Outline of Responsiveness score in severe traumatic brain injury patients. *Open Access Emerg. Med.* **Volume 9**, 69–72 (2017).
54. Naguib, A. N. *et al.* The Correlation of Two Cerebral Saturation Monitors With Jugular Bulb Oxygen Saturation in Children Undergoing Cardiopulmonary Bypass for Congenital Heart Surgery. *J. Intensive Care Med.* **32**, 603–608 (2017).
55. Vretzakis, G. *et al.* Cerebral oximetry in cardiac anesthesia. *J. Thorac. Dis.* **6 Suppl 1**, S60-9 (2014).
56. Murkin, J. M. & Arango, M. Near-infrared spectroscopy as an index of brain and tissue oxygenation. *Br. J. Anaesth.* **103**, i3–i13 (2009).
57. Lang, E. W. Continuous monitoring of cerebrovascular autoregulation: a validation study. *J. Neurol. Neurosurg. Psychiatry* **72**, 583–586 (2002).
58. Hogue, C. W. *et al.* Personalized Blood Pressure Management During Cardiac Surgery With Cerebral Autoregulation Monitoring: A Randomized Trial. *Semin. Thorac. Cardiovasc. Surg.* **33**, 429–438 (2021).
59. Masamoto, K. & Kanno, I. Anesthesia and the Quantitative Evaluation of Neurovascular Coupling. *J. Cereb. Blood Flow Metab.* **32**, 1233–1247 (2012).
60. Wood, M. D., Maslove, D. M., Muscedere, J. G., Day, A. G. & Gordon Boyd, J. Low brain tissue oxygenation contributes to the development of delirium in critically ill patients: A prospective observational study. *J. Crit. Care* **41**, 289–295 (2017).

61. Fischer, G. W. *et al.* Noninvasive cerebral oxygenation may predict outcome in patients undergoing aortic arch surgery. *J. Thorac. Cardiovasc. Surg.* **141**, 815–821 (2011).
62. Zheng, F. *et al.* Cerebral Near-Infrared Spectroscopy Monitoring and Neurologic Outcomes in Adult Cardiac Surgery Patients. *Anesth. Analg.* **116**, 663–676 (2013).
63. Baussart, B. *et al.* Multimodal cerebral monitoring and decompressive surgery for the treatment of severe bacterial meningitis with increased intracranial pressure. *Acta Anaesthesiol. Scand.* **50**, 762–765 (2006).
64. Citerio, G., Oddo, M. & Taccone, F. S. Recommendations for the use of multimodal monitoring in the neurointensive care unit. *Curr. Opin. Crit. Care* **21**, 113–119 (2015).
65. Thudium, M., Kornilov, E., Hilbert, T., Coburn, M. & Gestrich, C. Extended neuromonitoring in aortic arch surgery: A case series. *Anaesthesist* **70**, 68–73 (2021).
66. Michels, D. M., Van Dijk, L. C. & Tavy, D. L. J. Perioperative stroke during carotid endarterectomy: benefits of multimodal neuromonitoring - a case report. *BMC Neurol.* **22**, 325 (2022).
67. Elting, J. W. J., Tas, J., Aries, M. J. H., Czosnyka, M. & Maurits, N. M. Dynamic cerebral autoregulation estimates derived from near infrared spectroscopy and transcranial Doppler are similar after correction for transit time and blood flow and blood volume oscillations. *J. Cereb. Blood Flow Metab.* **40**, 135–149 (2020).

7 APPENDIX

7.1 EEG INFLUENCED BY ECC

Figure 18 illustrates the spectrogram of the EEG of patient 4. In figure 18b, the spectrogram during surgery is shown. As seen in this figure, during ECC a constant signal around 4Hz emerges. The power at 4 Hz is constant and within a narrow frequency band, indicating that it involves an artifactual signal. In order to pump the blood around the machine uses a frequency of approximately 4 Hz. Unfortunately, this signal could not be eliminated without distorting the EEG signal that we were interested in.

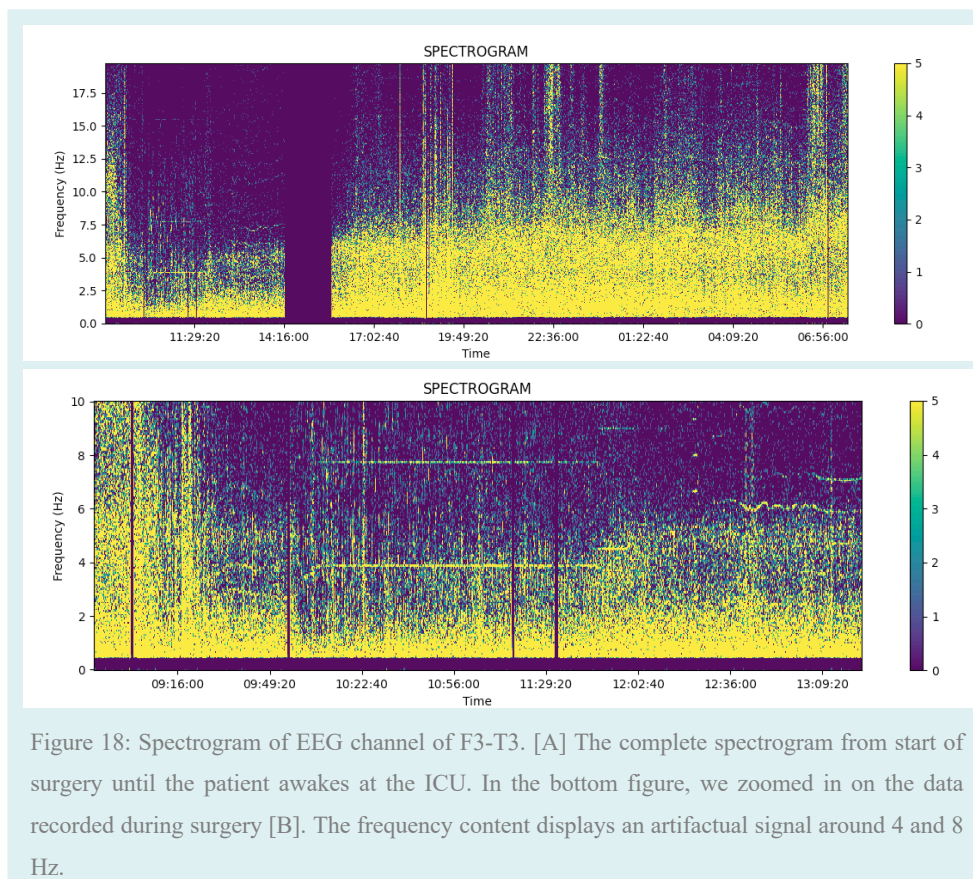


Figure 18: Spectrogram of EEG channel of F3-T3. [A] The complete spectrogram from start of surgery until the patient awakes at the ICU. In the bottom figure, we zoomed in on the data recorded during surgery [B]. The frequency content displays an artifactual signal around 4 and 8 Hz.